Expanding the Physics of Dark Matter

Exploring a new way to explain the acceleration of the Universe

Master of Science in Astrophysics

Written by *Karoline Løve and Kristine Simone Nielsen*

August 18, 2020

Supervised by
Steen H. Hansen

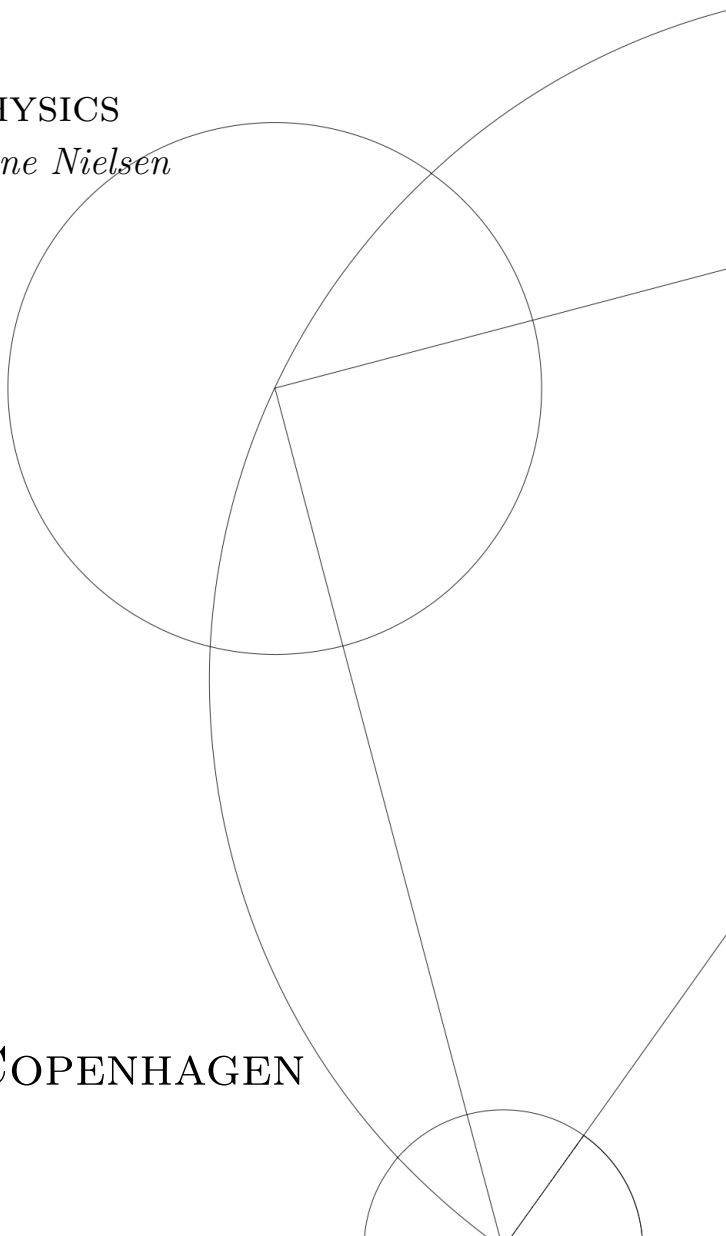

University of Copenhagen

UNIVERSITY OF COPENHAGEN

Name of Institute:	Niels Bohr Institute
Name of Department:	Dark Cosmology Centre
Authors:	Karoline Løve and Kristine Simone Nielsen
Email:	hlg223@alumni.ku.dk, qzk800@alumni.ku.dk
Title and subtitle:	Expanding the Physics of Dark Matter - Exploring a new way to explain the acceleration of the Universe
Supervisor:	Steen H. Hansen
Handed in:	18.08.2020
Defended:	

Name	Karoline Løve	Kristine Simone Nielsen
Signature	Karoline Løve	Kn
Date	18/08-2020	18/08-2020

Abstract

For more than 20 years, we have known that the Universe is accelerating in its expansion, which is caused by dark energy. The present theoretical explanation behind this is the cosmological constant, Λ, which is part of the current standard model of cosmology, known as the Benchmark model. However, it is possible to imagine other theoretical explanations for dark energy and the acceleration of the Universe. In this thesis we explore if it is possible to describe the acceleration of the Universe, through some effects of the movements of dark matter particles in dark matter halos. This model is based on the velocity dispersion of the halos, that is created due to the individual motions of the dark matter particles inside the halo. Through these motions of dark matter particles, an effect might arise that mimics the effects of Λ, which should enable us to substitute the cosmological constant in the Benchmark model. Using numerical simulations, we have tested possible variations of the model, where we find that our model provides a reasonable fit to the Benchmark model. This means that it is possible that our model is able to describe the acceleration of the Universe without including the cosmological constant.

Acknowledgements

First we would like to thank our brilliant supervisor Steen H. Hansen for his guidance and unlimited knowledge and patience with our numerous questions. We would especially like to thank him for always finding the time for us and being ready to meet and discuss problems whenever we needed it.

We would also like to thank Davide Martizzi and Troels Haugbølle for their help with the workings of RAMSES and numerical simulations. Davide helped introduce us properly to the program and guided us through the usual difficult beginning, when learning something new. Troels helped us while working with the simulations and allowed us to overcome our problems with the program that occurred during the process.

A last thank you goes to Rune Kildetoft for his patience when helping us with accessing and working with the HPC cluster.

Contents

1 Introduction

In this section we wish to go through the current understanding of the Universe and the observations that have led us to our modern viewpoint, in order to equip the reader with the needed background. We also present the idea behind our new model for the acceleration of the Universe, which is the main essence of this thesis.

1.1 The current understanding of the Universe

Through observations we know that the Universe consists of radiation, baryonic matter, dark matter and dark energy. The current common understanding of the Universe is known as the Benchmark model or the standard model of Big Bang cosmology. This describes a spatially flat universe containing radiation, baryonic matter, cold dark matter and a cosmological constant, Λ, which is a theoretical explanation of dark energy.[1] These have been measured in different ways and the effects of them have been observed through methods we will describe further on. When determining how much of our Universe is comprised of these different elements, we can describe them through the density parameter Ω, where these values are given by[2,3],

$$\Omega_{r,0} = 9 \cdot 10^{-5}, \quad \Omega_{m,0} = 0.31, \quad \Omega_{\Lambda,0} = 0.69, \tag{1.1.1}$$

where $\Omega_{r,0}$ is the density parameter of radiation, $\Omega_{m,0}$ is the density parameter of matter and $\Omega_{\Lambda,0}$ is the density parameter of dark energy. The zero subset indicates that these are the current values of the parameters. These parameters describe the ratio of the observed densities of the given components, to the critical density of the Universe, ρ_c.

$$\Omega_{x,0} = \frac{\rho_{x,0}}{\rho_{c,0}}, \tag{1.1.2}$$

where x can be either r, m or Λ and $\rho_{c,0}$ describes the density of a flat universe and can be found through,

$$\rho_{c,0} = \frac{3H_0^2}{8\pi G}, \tag{1.1.3}$$

where H_0 is the Hubble constant with a value of $H_0 = 67.66\,\mathrm{kms}^{-1}\mathrm{Mpc}^{-1}$ [4] and G is Newton's gravitational constant, $G = 6.67 \cdot 10^{-11}\,\mathrm{m}^3\mathrm{kg}^{-1}\mathrm{s}^{-2}$. $\rho_{c,0}$ has also been estimated through observations, where it is found by determining the density of a

[1] Coles, P. and Lucchin, F. 2002.
[2] Collaboration 2018.
[3] Ryden 2017.
[4] Collaboration 2018.

representative volume of the Universe. Through this, the Universe is confirmed to be flat with a critical density of about $8.7 \cdot 10^{-30}\,\mathrm{gm}^{-3}$.[5].

When determining the density parameters of the components of the Universe, the cosmic microwave background, CMB, is a useful tool. This is the electromagnetic radiation that was emitted at the early stages of the Universe and can be observed all over the sky. In Figure 1, a map of the density fluctuations in the CMB can be seen. This map consists of several small dots that together make up regions of either red or blue. These colors indicate the temperature and density of the areas, where the blue spots are colder and more dense regions and the red spots are warmer and less dense regions.[6]

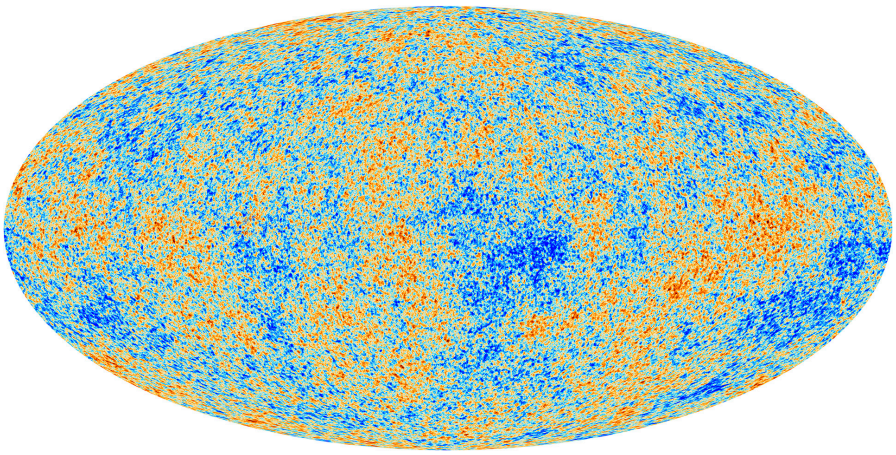

Figure 1: *A map of the cosmic microwave background, CMB.*[7]

The density of the radiation in our Universe is comprised of CMB radiation and is also thought to contain the theoretical cosmic neutrino background, CNB.[8] The density of the CMB radiation can be found directly from temperature measurements of the CMB, through the following equation[9,10],

$$\rho_{CMB,0} = \frac{4\sigma}{c^3} T_0^4, \tag{1.1.4}$$

where σ is the Stefan-Boltzmann constant, $\sigma = 5.67 \cdot 10^{-8}\,\mathrm{Jm}^{-2}\mathrm{s}^{-1}\mathrm{K}^{-4}$, c is the

[5]Ryden 2017.
[6]Freedman et al. 2014.
[8]Faessler et al. 2017.
[9]Dinculescu 2007.
[10]Fisenko, A. and Lemberg, V. 2014.

speed of light and T_0 is the temperature of the CMB today, $T_0 = 2.73$ K.[11] In order to find the density parameter of radiation, $\Omega_{r,0}$, as it is given in Equation (1.1.1), we use Equation (1.1.2), where we divide the density by the critical density of the Universe,

$$\Omega_{CMB,0} = \frac{\rho_{CMB,0}}{\rho_{c,0}} = 5.36 \cdot 10^{-5}. \tag{1.1.5}$$

The cosmic neutrino background corresponds to, $\Omega_{\nu,0} = 0.681 \cdot \Omega_{CMB,0}$[12], which means that the density of radiation in our Universe is,

$$\Omega_{r,0} = 1.681 \cdot \Omega_{CMB,0} = 9.01 \cdot 10^{-5}. \tag{1.1.6}$$

Contrary to radiation, the density parameter of matter and dark energy, cannot be determined from analysing the CMB alone. From CMB it is possible to determine the sum of the density parameters, Ω_{tot}, which is another way to confirm the geometry of the Universe. For a flat universe, this parameter should be equal to 1. In order to find this parameter, we look at the angular power spectrum of the CMB temperature anisotropies, that can be seen in Figure 2.

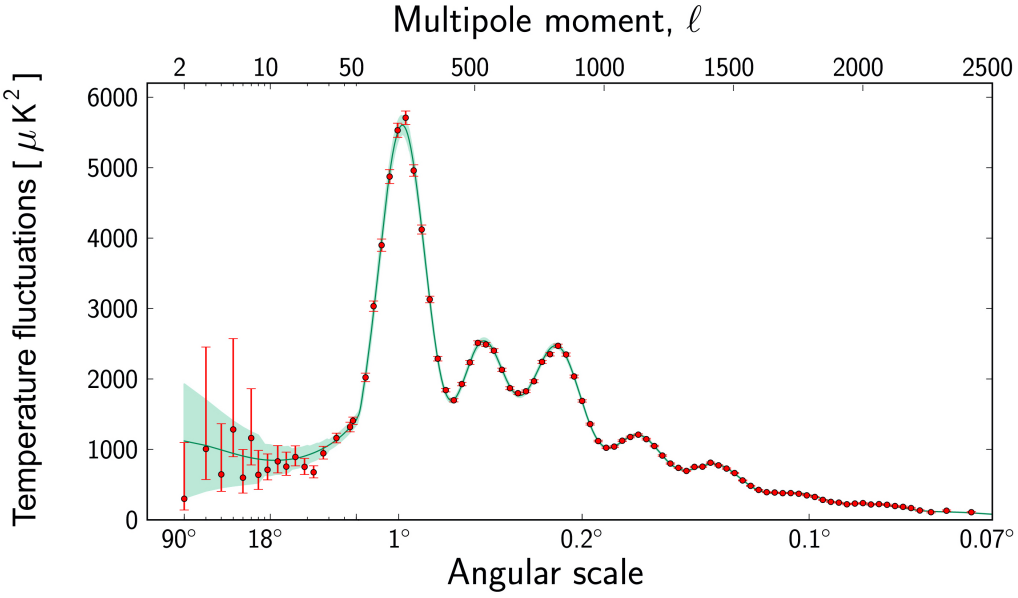

Figure 2: *The angular power spectrum of the CMB temperature anisotropies.*[13]

[11] Fisenko, A. and Lemberg, V. 2014.
[12] Birrell, J., Yang, C. T., and Rafelski, J. 2015.

In this figure, we see three large peaks centered at an angular scale of $\theta = 1°$, $\theta = 0.35°$ and $\theta = 0.25°$. The position of the peak tells us the apparent size of the density fluctuations in degrees, while the height of the peak tells us how many fluctuations are of this given size. From this, the position of the first peak tells us that we have an abundance of density fluctuations with an apparent size of $\theta = 1°$. From theoretical calculations, it has been shown that in order to have a flat universe, the average size of the density fluctuations, when CMB was emitted, had to be $\theta = 1°$. Had the Universe been open or closed, this value would have been different from $\theta = 1°$. Since a flat universe has a density parameter of $\Omega_{tot} = 1$, we know that the sum of the different density parameters have to be equal to 1, but we do not know the ratios of the individual parameters.[14]

From the power spectrum in Figure 2, we are able to find the ratio between the total amount of matter and baryons. This can be found by dividing the relative height of the first peak by the second peak, since the height of the first peak contains information about the amount of total matter and the second peak holds knowledge about the amount of baryons. If the two peaks were of an equal height, the ratio would be one and this would indicate that the matter of the Universe was only made up of baryons. There is a distinct difference in height between the two and therefore our Universe also contains matter that is not baryons, but instead dark matter. The ratio between the peaks reveals that there is 5 times more dark matter than baryons in the Universe.[15]

In order to determine the value of $\Omega_{m,0}$, one of the possible methods is to determine the total mass of matter of a certain area of the sky. Here, a representative region is chosen and the mass of all the galaxies and clusters within this volume is found. Since we now have a mass and volume, it is possible to find the density of matter and from this find the value of Ω_m.[16]

Another feature of the spectrum in Figure 2, is the rising of the curve in the far left side, which indicates the presence of dark energy in the Universe. Had the Universe been void of dark energy, this part of the curve would have been flat, in fact if all perturbations in the early Universe had been distributed evenly size-wise, the entire power spectrum would have been flat. However, as the perturbations have evolved, an abundance of certain sizes has emerged, which we see through the peaks of the spectrum. The large structures had not yet been created at the

[14] Freedman et al. 2014.
[15] de Bernardis et al. 2002.
[16] Allen et al. 2003.

time of CMB emission and we would therefore expect the left part of the spectrum to be flat. Instead we see that this part is slightly raised, which is caused by the photons traveling through an accelerating universe, indicating the presence of dark energy.[17] However, when determining the density of dark energy, it is not enough to only look at observations of the CMB and the power spectrum. Instead, observations of both supernovae or baryonic acoustic oscillations are needed.

When scientists were analysing distant supernovae type Ia, they discovered a correlation when looking at their redshifts and observed magnitudes, that can be seen in Figure 3. By fitting models of different universes to this correlation, e.g. an empty universe and a universe with and without dark energy, they saw that the best fit was a universe with the parameters $\Omega_{m,0} \simeq 0.3$ and $\Omega_{\Lambda,0} \simeq 0.7$, which helps strengthen the theory that we live in an accelerating universe.[18] However, since the measurements of the supernovae contain uncertainties, it is necessary to use observations of other parts of the Universe, before we can draw a conclusion of these values.

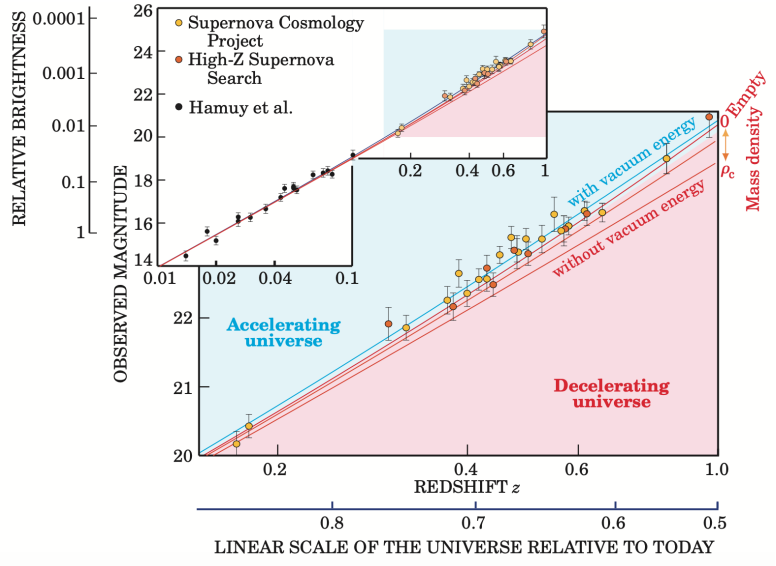

Figure 3: *A plot of observed magnitudes against redshifts of distant type Ia supernovae.*[19]

[17] Weller, J. and Lewis, A. M. 2003.
[18] Perlmutter 2000.

Baryonic acoustic oscillations, BAO, are used for measuring how the expansion rate of the Universe has changed over time and this in turn makes it possible to constrain the values of the cosmological parameters even further. These oscillations in the density of the visible baryonic matter stem from perturbations in the early universe, which we also observed through the CMB. From the first peak of the CMB power spectrum, a characteristic size of the fluctuations was revealed. By observing galaxies and the distances between them at different redshifts, we can examine whether this size is consistent with the size found from the power spectrum. This scale was determined by the fluctuations in the early Universe and by calculating how this characteristic scale evolves over time, it is possible to see if the distances between the galaxies at different redshifts correspond with this size. By measuring this scale during the accelerating expansion, as opposed to the time where the CMB was emitted, we are able to determine the same characteristics through two different methods.[20]

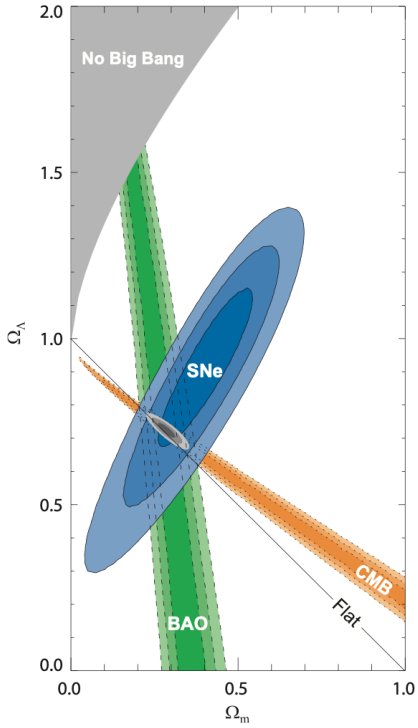

Figure 4: *Contours of the ranges of the values of the cosmological parameters for matter and dark energy found through analysing supernovae, baryonic acoustic oscillations and the cosmic microwave background.*[21]

[20] **BAO**.

Combining all these measurements, CMB, supernovae and BAO, we are able to find a fairly precise estimate of the value of the cosmological parameters for matter and dark energy. By looking at Figure 4, we see the range of the values for the parameters found through the different methods. The contours correspond to confidence levels of 68.3%, 95.4% and 99.7%. By combining all three ranges, the grey contour in the middle is found, which gives us a small and precise span for the values of the cosmological parameters, corresponding to values of $\Omega_{m,0} = 0.285^{+0.022}_{-0.022}$ and $\Omega_{\Lambda,0} = 0.713^{+0.045}_{-0.041}$.[22]

1.2 Structure formation

During the lifetime of the Universe, its components have gathered and formed in different kinds of structures of varying sizes and physical traits. The Big Bang theory suggests that shortly after the beginning, the Universe consisted of a smooth distribution of dark matter in which quantum fluctuations caused the dark matter to create potential wells into which the dark and visible matter could congregate. These are the same fluctuations as those in the CMB map in Figure 1, where the blue regions indicate the areas with higher density and deepest potential wells.[23]

The potential wells are also what underlie the weblike structure we see, when looking at the distribution of matter in our Universe on large scales today, as can be seen in Figure 5. Here, each black dot is a galaxy and as the redshift decreases and the matter congregates, these galaxies are located primarily in clusters and threads of galaxies connecting these clusters. In between them, in the white areas, are voids of empty space.[24]

[22] Kowalski et al. 2008.
[23] Freedman et al. 2014.
[24] Sparke, L. S. and Gallagher III, J. S. 2007.

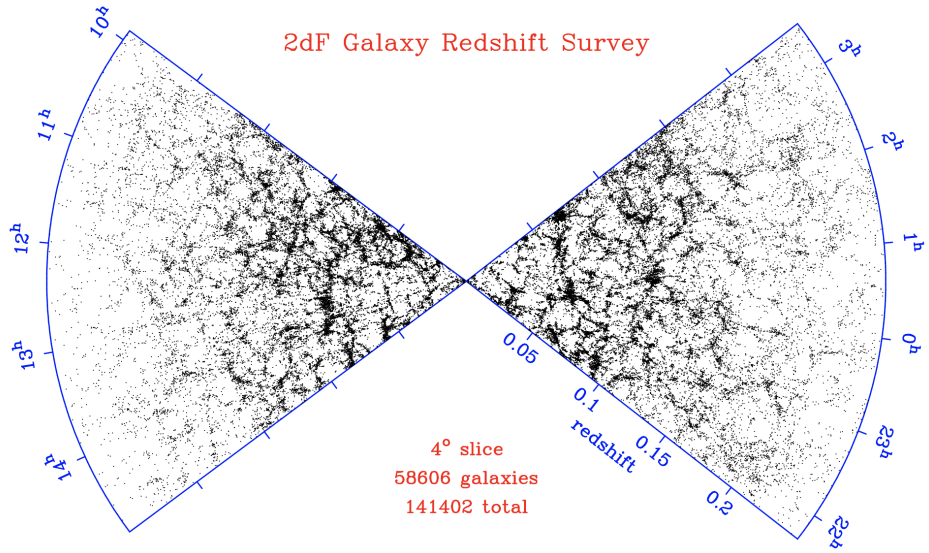

Figure 5: *The distribution of galaxies in the Universe showing the Large Scale Structure.*[25]

The clusters of dark matter are known as dark matter halos in which galaxies can be located in the centre. Over time, these dark matter halos grow by accreting mass from nearby areas or merging with other dark matter halos, creating increasingly bigger halos and structures. These dark matter halos are significant for the work of our thesis and will be brought up again later on.

1.3 Evolution of the Universe

Many different types of universes, with varying cosmological parameters, have been explored in the pursuit of finding the true nature of our own. In Figure 6 some of these models can be seen. These different universes diverge in many directions, which make the future and past of the Universe vary depending on which model we look at. The blue, green and orange curves all show matter-only universes, but the value of the density parameter varies. For the orange curve, the sum of the density parameters is $\Omega_{tot} > 1$, which makes it a closed universe. This type of universe will expand at first, but then at one point in its lifetime, it will reach a maximum size and then start to contract. The blue curve shows the case of an open universe where the sum of the density parameters is $\Omega_{tot} < 1$, and this type of universe will keep expanding forever. The green curve is a flat universe with $\Omega_{tot} = 1$, like our own. In this universe the expansion will slowly start to slow down due to the gravitational pull of matter. Lastly, the purple curve shows

a flat universe containing both matter and the cosmological constant, where the expansion of the universe will accelerate and continue forever.[26]

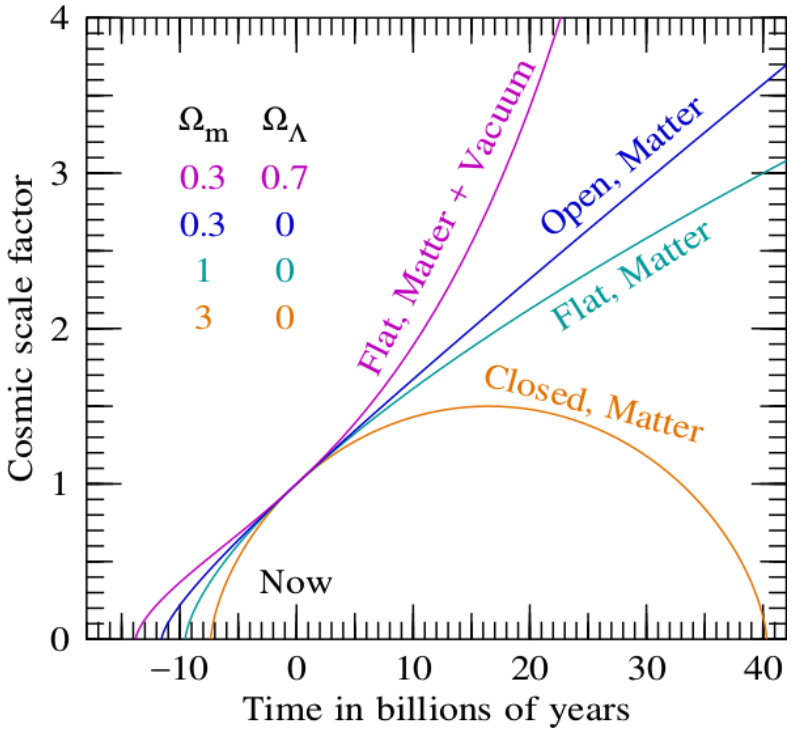

Figure 6: *The evolution of several types of universes with differing cosmological parameters.*[27]

Several observations have supported the existence of dark energy, and the theoretical model containing the cosmological constant, Λ, seems to be the best fit, as shown in the previous section. The future of the evolution of the Universe, should therefore follow the purple curve, according to this theory. However, there are many unknown features of dark energy and it is possible to imagine other theoretical explanations for this and thereof the acceleration of the Universe, which do not involve the cosmological constant.

1.4 Our proposed model

We are interested in exploring a universe like the Benchmark model, but without the cosmological constant. In this universe, the effects of the acceleration of the Universe would have to be explained by some new theory of the workings of dark

[26] Ryden 2017.

matter. This would mean, that instead of having two fundamentally different components of the Universe, that we know very little about, we would now instead have just one unknown component, but one which we would know the physics of the forces behind. To understand our new force we start by looking at the physics behind electromagnetic forces.

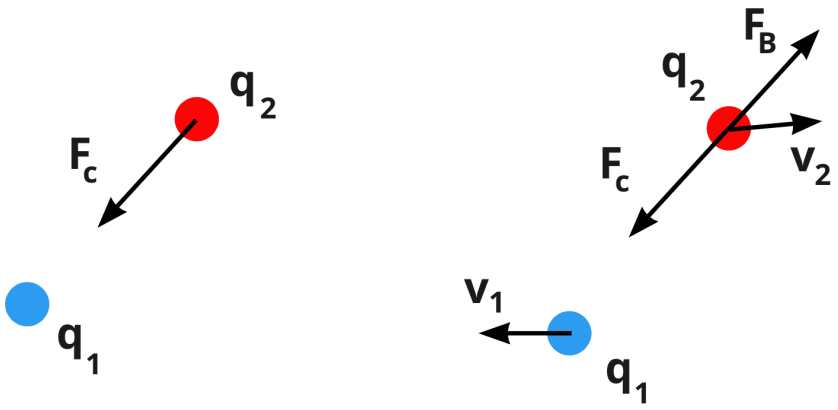

Figure 7: *A simple drawing of the basics of electromagnetism.*

In Figure 7, a simple drawing of the basics of electromagnetism is shown. In the left side of the figure, two stationary electrically charged particles can be seen, q_1 (blue) and q_2 (red). Focusing on q_2, this feels the electric force that arises between the two particles, the Coulomb force, F_c, which depends on the charge of the particles and the distance between them.[28] In the right side of the figure the same electrically charged particles are visible, but in this scenario the two particles move with two different velocities, v_1 and v_2. The Coulomb force is still present, and due to the movement of the particles, a magnetic force appears called the Lorentz force, F_B, which, among others, depends on the velocity of the particles.[29]

Likewise, we can imagine a different force also depending on the velocity, which is illustrated in Figure 8. In the left side of this figure, two groups of stationary non-charged particles, described through the yellow and the green dot, attract each other due to their masses. Because of this, the yellow dot feels a gravitational force, F_G, from the green dot, and vice versa. If we then imagine that the green dot has a velocity dispersion, σ^2, since the particles within the group move around in different directions with varying velocities, we get the case in the right side of the figure. Here, a new force could appear due to the velocity dispersion, like in the

[28] Griffiths 2013.
[29] Ibid.

electromagnetic example, where the Lorentz force occurs because of the movement of the charged particles. This new force, F_{New}, could be a repulsive force and therefore be opposite of the gravitational force, F_G, as shown in the figure.

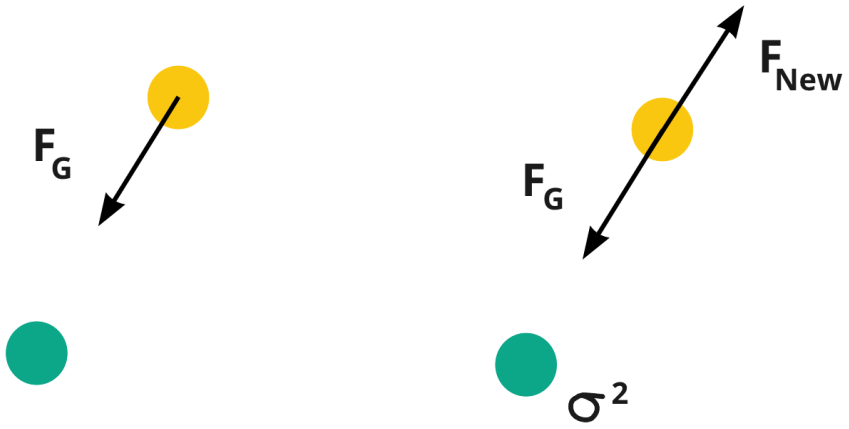

Figure 8: *A simple drawing of the idea behind our new force.*

As mentioned above, we wish to look at a universe, without the cosmological constant, Λ. In the left side of Figure 9, the Benchmark model is shown, where the Universe contains both the cosmological constant and matter. Here, a group of dark matter particles on the edge of a sphere will feel a gravitational force, F_G, from the matter within this sphere and a repulsive force, F_Λ, due to the acceleration of the Universe caused by the cosmological constant. In the right side of the figure, a universe without the cosmological constant can be seen. Here, the group of dark matter particles on the edge of the sphere still feel a gravitational force from the other groups within the sphere, and like in the simple case from Figure 8, we imagine that a new repulsive force, now called F_{DM}, can arise due to the velocity dispersion of the dark matter groups within the sphere. The subscript DM in our new force, denotes that it stems from dark matter. This force could in this scenario be the cause of the acceleration of the Universe.

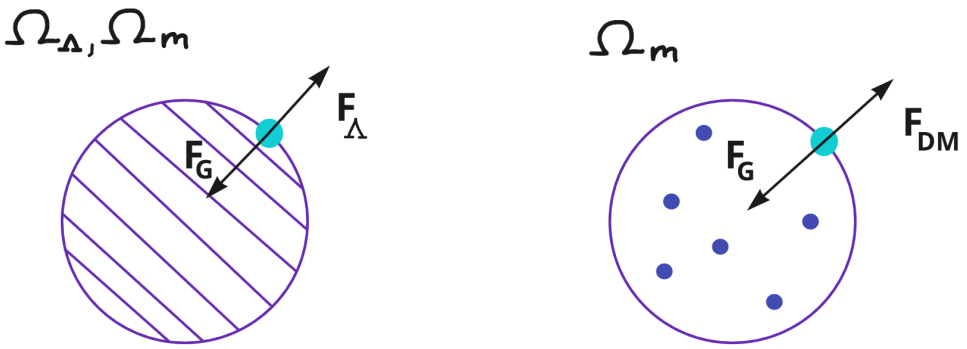

Figure 9: *A drawing of the forces of the Benchmark model (left) along with the possible forces of a universe without the cosmological constant (right).*

2 Theory

In this section, we derive an equation for the acceleration of the Universe according to the Benchmark model, using the Friedmann, fluid and acceleration equation. This equation is later used as a comparison for our own model. We will also describe the theory behind our new model, where we introduce a specific equation for this. Lastly, we go over the theory of numerical simulations, along with an introduction to the RAMSES project[30] and MUSIC[31], which were both used for creating a simulation in this thesis.

2.1 Acceleration of the Universe

The expansion of the Universe can be described using the Friedmann equation, which is a statement of energy conservation in a Newtonian approximation. Even though the Friedmann equation is a very important equation in cosmology, we also need other equations, such as the fluid equation, the acceleration equation and the equation of state, in order to describe and understand the expansion of the Universe. In the following sections the different equations will be derived and explained.

When deriving the Friedmann equation, the correct way is to do this using general relativity. However, for the purpose of this thesis, we can simplify the case using a Newtonian approximation. This is done in order to make it easier to understand the physics behind the Friedmann equation and thereby making the theory behind our proposed model more clear.

In the following subsections, the approach and derivations of Barbara Ryden in *Introduction to Cosmology*[32] are used for guidance.

2.1.1 The Friedmann equation

The Friedmann equation can be derived from Newtonian physics by looking at the expansion or contraction of the Universe. We start from Newton's law of gravity and second law of motion, where we consider a homogeneous sphere of matter with a total mass M, which is constant with time, as can be seen in Figure 10. The sphere is expanding or contracting isotropically, so that its radius $R(t)$ is increasing or decreasing with time. If we place a test mass m on the surface of the sphere, the

[30] Teyssier 2002.
[31] Hahn, O. and Abel, T. 2011.
[32] Ryden 2017.

gravitational force felt by the test mass will be given by Newtons' law of gravity,

$$F = -\frac{GMm}{R(t)^2}. \tag{2.1.1}$$

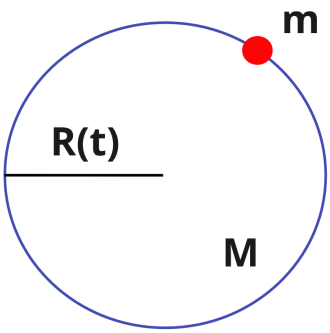

Figure 10: *An expanding or contracting sphere with a radius $R(t)$ and mass M, along with a test mass, m, on the surface of the sphere.*

The gravitational acceleration at the surface of the sphere is given by Newton's second law of motion,

$$\frac{d^2R}{dt^2} = -\frac{GM}{R(t)^2}. \tag{2.1.2}$$

Multiplying each side with dR/dt and integrating, we get,

$$\begin{aligned} &\int \frac{dR}{dt}\frac{d^2R}{dt^2} = -\int \frac{GM}{R(t)^2}\frac{dR}{dt} \Leftrightarrow \\ &\int \frac{dR}{dt}\frac{d^2R}{dt^2}\,dt = -GM\int \frac{1}{R(t)^2}\,dR \Leftrightarrow \\ &\frac{1}{2}\left(\frac{dR}{dt}\right)^2 = \frac{GM}{R(t)} + U, \end{aligned} \tag{2.1.3}$$

where U is a constant of integration.

From Equation (2.1.3), we can define the kinetic energy per unit mass, E_{kin}, and the potential energy per unit mass, E_{pot}, as,

$$E_{kin} = \frac{1}{2}\left(\frac{dR}{dt}\right)^2 \quad \text{and} \quad E_{pot} = -\frac{GM}{R(t)}. \tag{2.1.4}$$

Defining these two expressions for E_{kin} and E_{pot}, Equation (2.1.3) now states that the sum of the kinetic energy per unit mass, E_{kin}, and the potential energy per unit mass, E_{pot}, is constant at the surface of the sphere, while the sphere is expanding or contracting due to self-gravity.

The mass of the sphere can be defined as,

$$M = \frac{4}{3}\pi\rho(t)R(t)^3, \tag{2.1.5}$$

since the mass is constant.

Inserting the expression for M in Equation (2.1.3) we get,

$$\frac{1}{2}\left(\frac{dR}{dt}\right)^2 = \frac{4\pi G}{3}\rho(t)R(t)^2 + U. \tag{2.1.6}$$

Rewriting dR/dt as $\dot{R}$, we get the Friedmann equation in its Newtonian form,

$$\begin{aligned} &\frac{1}{2}\left(\dot{R}\right)^2 = \frac{4\pi G}{3}\rho(t)R(t)^2 + U \Leftrightarrow \\ &\left(\frac{\dot{R}}{R}\right)^2 = \frac{8\pi G}{3}\rho(t) + \frac{U}{R(t)^2}. \end{aligned} \tag{2.1.7}$$

Usually one derives the Friedmann equation in terms of the dimensionless scale factor, a, which is defined as $R(t) = a(t) \cdot r$, where r is a comoving radius. But since we are interested in physical units, we have chosen not to derive it in terms of the scale factor, but instead in terms of the radius of the expanding or contracting sphere, R.

Looking at an expanding sphere, $\dot{R} > 0$, we can consider three possible cases, depending on the sign of U. The first case is $U > 0$, where the right-hand side of Equation (2.1.7) is always positive and therefore $\dot{R}$ is always positive. In this case the expansion of the sphere will never stop, corresponding to an open universe. The second case is $U < 0$, where the right-hand side of Equation (2.1.7) starts out being positive, but will turn zero at a maximum radius, $R_{max} = -GM/U$. After this $\dot{R}$ will be negative, and the sphere will start to contract, as is the case for a closed universe. The third case is $U = 0$, which is the boundary case in which $\dot{R} \to 0$, as $t \to \infty$ and $\rho \to 0$. This means that the expansion of the sphere will eventually stop as the density of the matter decreases with time.

We know from observations stated in Section 1.1, that our Universe is almost spatially flat, which corresponds to the third case, where $U = 0$. The sphere mentioned above only contains matter, but according to the Benchmark model, the Universe also contains radiation and dark energy. Therefore, we wish to rewrite the Friedmann equation, so that it fits with the components of the Universe. We do this by writing the Friedmann equation in terms of energy density, ε, instead of matter density, ρ. The energy density is given by $\varepsilon = \rho c^2$. Inserting this in Equation (2.1.7), we get the final edition of the Friedmann equation,

$$\left(\frac{\dot{R}}{R}\right)^2 = \frac{8\pi G}{3c^2}\varepsilon(t). \tag{2.1.8}$$

2.1.2 The Fluid equation

In the Friedmann equation, given by Equation (2.1.8), we have two unknown parameters, $R(t)$ and ε. We therefore need to derive another equation which contains these two parameters, in order to be able to find the value of these. This equation is known as the fluid equation. Since the Friedmann equation describes energy conservation, we start by looking at another case of energy conservation in the first law of thermodynamics,

$$dQ = dE + PdV, \tag{2.1.9}$$

where dQ is the heat flow in or out of a volume, dE is the change in internal energy, P is the pressure and dV is the change in volume.

A perfectly homogeneous universe, where there is no heat flow, can be described through an adiabatic process, which means that $dQ = 0$. This leads us to the following version of the equation,

$$0 = \dot{E} + P\dot{V}. \tag{2.1.10}$$

When we derived the Friedmann equation, we took as a starting point, that we were looking at a spherical section of the Universe, as seen in Figure 10. To continue with this reference point, we can use the differentiated volume of the given sphere to insert into Equation (2.1.10).

The volume of a sphere is given by,

$$V(t) = \frac{4\pi}{3}R(t)^3. \tag{2.1.11}$$

The differentiated volume is then,

$$\dot{V} = \frac{4\pi}{3} 3R(t)^2 \dot{R}. \tag{2.1.12}$$

If we decide to divide and multiply with $R(t)$, the equation becomes,

$$\dot{V} = \frac{4\pi}{3} 3R(t)^3 \frac{\dot{R}}{R(t)}, \tag{2.1.13}$$

where we recognise the expression for $V(t)$. The final differentiated volume is then,

$$\dot{V} = V(t) \cdot 3\frac{\dot{R}}{R(t)}. \tag{2.1.14}$$

Next, we look at the expression for $E(t)$, which was the internal energy. For a sphere this is given as,

$$E(t) = V(t)\varepsilon(t), \tag{2.1.15}$$

where $\varepsilon(t)$ is the energy density.

In order to see the change in internal energy, we differentiate this,

$$\dot{E} = \dot{V}\varepsilon(t) \cdot V(t)\dot{\varepsilon} = \left(V(t) \cdot 3\frac{\dot{R}}{R(t)} \right) \varepsilon(t) + V(t)\dot{\varepsilon}. \tag{2.1.16}$$

We can now insert Equation (2.1.14) and (2.1.16) into Equation (2.1.10).

$$\begin{aligned} 0 &= V(t) \cdot 3\frac{\dot{R}}{R(t)}\varepsilon(t) + V(t)\dot{\varepsilon} + PV(t) \cdot 3\frac{\dot{R}}{R(t)} \\ &= V(t) \left(3\frac{\dot{R}}{R(t)}\varepsilon(t) + \dot{\varepsilon} + P \cdot 3\frac{\dot{R}}{R(t)} \right). \end{aligned} \tag{2.1.17}$$

Since the volume of a sphere can't be equal to zero, we know that the product of the parenthesis must be zero in order for the equation to be true. In the following equation we look only at the terms inside of the parenthesis.

$$0 = 3\frac{\dot{R}}{R(t)}\varepsilon(t) + \dot{\varepsilon} + P \cdot 3\frac{\dot{R}}{R(t)} = 3\frac{\dot{R}}{R(t)}(\varepsilon(t) + P) + \dot{\varepsilon}. \tag{2.1.18}$$

Rewriting this, we get the fluid equation,

$$\dot{\varepsilon}\frac{R(t)}{\dot{R}} = -3(\varepsilon(t) + P). \tag{2.1.19}$$

2.1.3 The Acceleration equation

With both the Friedmann equation and the fluid equation, we are finally able to find the acceleration equation. This describes the acceleration of the Universe and is useful when looking at the evolution of it. To derive the acceleration equation, we start by taking the time derivative of the Friedmann equation,

$$\begin{aligned} &\frac{d}{dt}\dot{R}^2 = \frac{8\pi G}{3c^2}\frac{d}{dt}\varepsilon(t)R^2(t) \Leftrightarrow \\ &\ddot{R}\dot{R} + \dot{R}\ddot{R} = \frac{8\pi G}{3c^2}\left(\dot{\varepsilon}R(t)^2 + \varepsilon(t)\dot{R}R(t) + \varepsilon(t)R(t)\dot{R}\right). \end{aligned} \tag{2.1.20}$$

By reducing this equation we get,

$$2\ddot{R}\dot{R} = \frac{8\pi G}{3c^2}\left(\dot{\varepsilon}R(t)^2 + 2\varepsilon(t)\dot{R}R(t)\right). \tag{2.1.21}$$

We now decide to divide both sides of this equation with $2\dot{R}R(t)$,

$$\frac{\ddot{R}}{R(t)} = \frac{4\pi G}{3c^2}\left(\dot{\varepsilon}\frac{R(t)}{\dot{R}} + 2\varepsilon(t)\right). \tag{2.1.22}$$

The first term in the parenthesis can be recognised as the fluid equation. When inserting this, the equation then becomes,

$$\begin{aligned} \frac{\ddot{R}}{R(t)} &= \frac{4\pi G}{3c^2}\left(-3(\varepsilon(t) + P) + 2\varepsilon(t)\right) \\ &= \frac{4\pi G}{3c^2}\left(-\varepsilon(t) - 3P\right) = -\frac{4\pi G}{3c^2}\left(\varepsilon(t) + 3P\right). \end{aligned} \tag{2.1.23}$$

This equation can be rewritten using the equation of state, $P = w\varepsilon$, which is a linear relation between the pressure and the energy density, where w is a dimensionless number. Using this we get the acceleration equation in its final form,

$$\frac{\ddot{R}}{R(t)} = -\frac{4\pi G}{3c^2}\varepsilon(t)\left(1 + 3w\right). \tag{2.1.24}$$

2.1.4 The Benchmark model

We can now describe the acceleration of the Universe using Equation (2.1.24) by inserting the components of the Universe. According to the Benchmark model, the Universe contains radiation, matter (both baryonic and cold dark matter) and the cosmological constant, Λ. We can therefore rewrite the acceleration equation by inserting the energy densities of these different components.

The energy density of matter and radiation is given by,

$$\begin{aligned} \varepsilon_m &= \varepsilon_{m,0} a^{-3} = \varepsilon_{m,0}(1+z)^3, \\ \varepsilon_r &= \varepsilon_{r,0} a^{-4} = \varepsilon_{r,0}(1+z)^4, \end{aligned} \tag{2.1.25}$$

where $\varepsilon_{m,0}$ and $\varepsilon_{r,0}$ is the energy density of matter and radiation today. Rewriting these in terms of physical units using $R(t) = a(t) \cdot r$, we get,

$$\varepsilon_m = \varepsilon_{m,0} \left(\frac{R}{r}\right)^{-3}, \quad \varepsilon_r = \varepsilon_{r,0} \left(\frac{R}{r}\right)^{-4}. \tag{2.1.26}$$

The energy density of the cosmological constant, Λ, is constant, meaning that $\varepsilon_\Lambda = \varepsilon_{\Lambda,0}$, where $\varepsilon_{\Lambda,0}$ is the energy density of cosmological constant today. Each component has a different equation of state parameter, w. For matter the parameter is $w = 0$, for radiation it is $w = \frac{1}{3}$, and for the cosmological constant the parameter is $w = -1$.

At first we rewrite the acceleration equation (2.1.24) in terms of the critical energy density of the Universe today, $\varepsilon_{c,0}$, and the Hubble constant, H_0. The critical energy density of the Universe today is given by,

$$\varepsilon_{c,0} = \frac{3c^2}{8\pi G} H_0^2. \tag{2.1.27}$$

Inserting this in Equation (2.1.24) gives us,

$$\begin{aligned} \frac{\ddot{R}}{R} &= -\frac{4\pi G}{3c^2} \varepsilon (1+3w) \Leftrightarrow \\ \frac{\ddot{R}}{R} &= -\frac{H_0^2}{2\varepsilon_{c,0}} \varepsilon (1+3w). \end{aligned} \tag{2.1.28}$$

Inserting the energy densities and the equation of state parameters of the different components we get,

$$\begin{aligned} \frac{\ddot{R}}{R} &= -\frac{H_0^2}{2\varepsilon_{c,0}} (\varepsilon_m(t) + 2\varepsilon_r(t) - 2\varepsilon_\Lambda(t)) \Leftrightarrow \\ \frac{\ddot{R}}{R} &= -\frac{H_0^2}{2\varepsilon_{c,0}} \left(\varepsilon_{m,0} \left(\frac{R}{r}\right)^{-3} + 2\varepsilon_{r,0} \left(\frac{R}{r}\right)^{-4} - 2\varepsilon_{\Lambda,0} \right). \end{aligned} \tag{2.1.29}$$

We can rewrite $\varepsilon_{x,0}$ in terms of the density parameter, $\Omega_{x,0}$, which is given by $\Omega_{x,0} = \varepsilon_{x,0}/\varepsilon_{c,0}$. Inserting this gives us,

$$\frac{\ddot{R}}{R} = -\frac{H_0^2}{2}\left(\Omega_{m,0} r^3 R^{-3} + 2\Omega_{r,0} r^4 R^{-4} - 2\Omega_{\Lambda,0}\right). \tag{2.1.30}$$

Isolating the acceleration, $\ddot{R}$, we get,

$$\ddot{R} = -\frac{H_0^2}{2}\left(\Omega_{m,0} r^3 R^{-2} + 2\Omega_{r,0} r^4 R^{-3} - 2\Omega_{\Lambda,0} R\right). \tag{2.1.31}$$

From this equation we are now able to describe the acceleration of the Universe according to the Benchmark model and understand how the Universe evolves over time. At different times in the history of the Universe, the different components dominate, as can be seen in Figure 11, which shows the scale factor as a function of time. In the early Universe, until $z \simeq 3600$, radiation dominated the acceleration of the Universe, afterwards matter dominated the acceleration until $z \simeq 0.6$, and now the cosmological constant, Λ, dominates the acceleration, leaving us with a inflationary-like epoch. These different epochs are contained in the acceleration equation, which we know describes the seen evolution of the Universe.

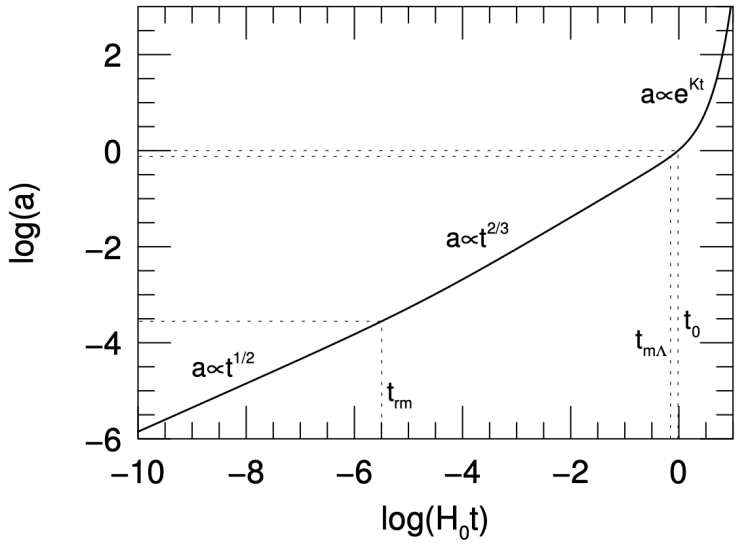

Figure 11: *The scale factor as a function of time for the Benchmark model. The dashed lines indicate the transition between the different epochs of the Universe.*[33]

In our thesis, we are interested in being able to describe the acceleration of the Universe without Λ, but we still need for our model to support the expansion we see today. The acceleration equation describes the acceleration of the Universe as it is observed today, which makes it a good comparison model, when testing whether our new model can be used as an alternative theory to describe the acceleration of the Universe. In order to see deviations between our new model and the acceleration equation, we look at the *normalised acceleration*, since it is easier to see variations and small details. We get the normalised acceleration by dividing the acceleration of the Universe, $\ddot{R}$, given by Equation (2.1.31), with the acceleration of the Universe in the matter dominated epoch, $\ddot{R}_{m,analytical}$. This component is locked by the fact that there is a given amount of matter in the Universe, which makes it a fixed variable to divide it by. The acceleration of the Universe in the matter dominated epoch is given by,

$$\ddot{R}_{m,analytical} = -\frac{H_0^2}{2}\Omega_{m,0} r^3 R^{-2}. \tag{2.1.32}$$

By dividing $\ddot{R}$ by $\ddot{R}_{m,analytical}$, we get the normalised analytical acceleration, which we will use as a comparison for our new model.

$$\ddot{R}_{norm} = \frac{\ddot{R}}{\ddot{R}_{m,analytical}} = 1 + 2\frac{\Omega_{r,0}}{\Omega_{m,0}} r^1 R^{-1} - 2\frac{\Omega_{\Lambda,0}}{\Omega_{m,0}} r^{-3} R^3. \tag{2.1.33}$$

2.2 The potential forces of dark matter

2.2.1 Possible scenario

According to the Benchmark model, we are currently in a phase where the cosmological constant, Λ, dominates, resulting in an accelerating and rapidly expanding universe. We still know very little about Λ and the cause of this, but it is theorised to be a kind of vacuum energy, meaning that the more space that arises in between objects, the greater the effects of the cosmological constant we will see.[34] The acceleration of the Universe will therefore only grow in the future, so if we look at the normalised acceleration this should decrease as can be seen in Equation (2.1.33).

In Figure 12 the normalised acceleration can be seen as the solid black line. At the beginning, the curve depicts the matter dominated universe, making it start at $\ddot{R}/\ddot{R}_m = 1$. From there, the cosmological constant starts to dominate, making the curve decrease rapidly due to the negative Λ-term in Equation (2.1.33).

[34] Kragh 2011.

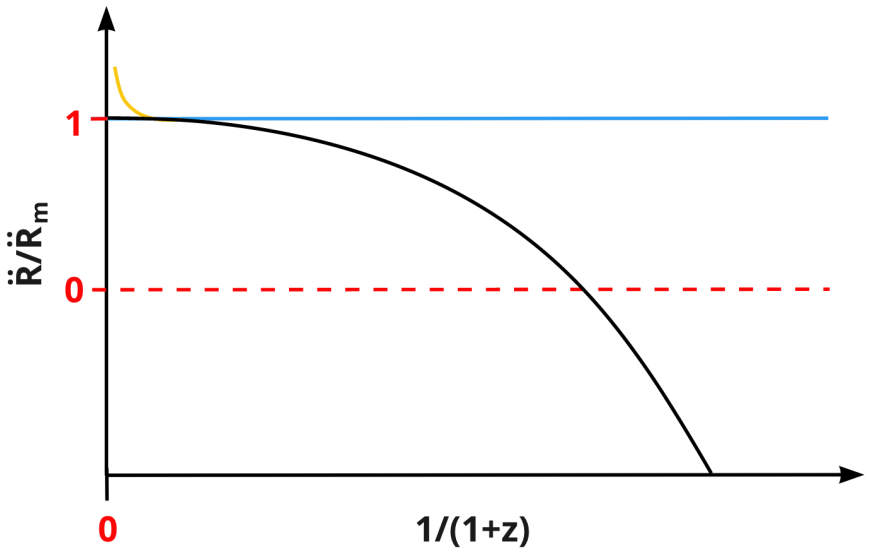

Figure 12: *The normalised analytical acceleration as a function of* $1/(1+z)$ *for the Benchmark model (black), a matter-only universe (blue) and a matter-radiation universe (orange) which follows the blue line after the rapid decrease.*

In order to make the normalised acceleration more clear, the evolution of the curve for a matter-only universe can be seen as the constant, blue line, where $\ddot{R}/\ddot{R}_m = 1$. The orange line shows the matter-radiation universe, where it starts off at $\ddot{R}/\ddot{R}_m > 1$ and then decreases rapidly, after which it follows the blue line at $\ddot{R}/\ddot{R}_m = 1$. In reality the orange line is only slightly above one in the beginning. It has been exaggerated in this figure, in order to make it more visible.

If the force responsible for the acceleration of the Universe was not due to vacuum energy and the cosmological constant, but instead due to the movement of dark matter particles, we would be looking at a different cosmology, where the cosmological constant is no longer needed. We propose a new explanation for dark energy and the acceleration of the Universe, where we calculate this from the velocity dispersions of dark matter halos. When dark matter particles are moving around in their respective halos, a force can arise similar to the Lorentz force, as already explained. As the halos grow bigger, their velocity dispersions increase, in turn resulting in a greater force. During the evolution of the Universe, structures have formed and grown, making the force increase over time. This could cause the expansion of the Universe to accelerate, as the force grows stronger. However, in the future we will reach a point where structure formation stops, consequently making the force constant.[35] The Universe will then continue expanding at a constant rate.

[35]Ryden 2017.

This scenario can be seen in Figure 13 as the green line.

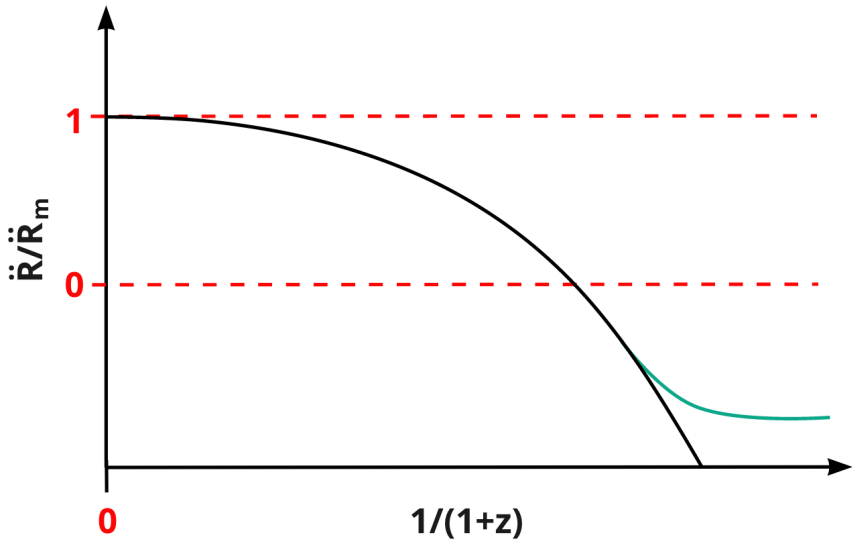

Figure 13: *The normalised analytical acceleration as a function of* $1/(1+z)$ *for the Benchmark model (black) along with a new possible scenario (green).*

The evolution of structure formation depends on the small density perturbations in matter, that were explained in Section 1.2, and how these have grown over time in the different epochs of the Universe. To see how the density perturbations grow in an expanding universe, we can look at the following equation[36],

$$\ddot{\delta} + 2H\dot{\delta} - \frac{3}{2}\Omega_m H^2 \delta = 0, \tag{2.2.1}$$

where $|\delta| \ll 1$ and is the amplitude of the density perturbations in matter and H is the Hubble parameter, given by $H = \dot{a}/a$. The second term of the equation is known as the Hubble friction and this is the term that causes the slowing of the growth of the density perturbations in an expanding universe, making the structure formation slower.

In the radiation dominated epoch, the density parameter of matter is very small, $\Omega_m(z) = \Omega_{m,0}/(1+z)^3 \ll 1$, which makes it negligible. The Hubble parameter in this epoch is $H = 1/(2t)$, so Equation (2.2.1) is reduced to the following equation and its corresponding solution,

$$\ddot{\delta} + \frac{1}{t}\dot{\delta} \approx 0 \quad \Rightarrow \quad \delta(t) \approx B_1 + B_2 \ln(t), \tag{2.2.2}$$

[36]Ryden 2017.

where B_1 and B_2 depend on the initial conditions for $\delta(t)$. From this equation we see, that the density perturbations grow at a logarithmic scale, which results in a slow growth, as can be seen in Figure 14a.

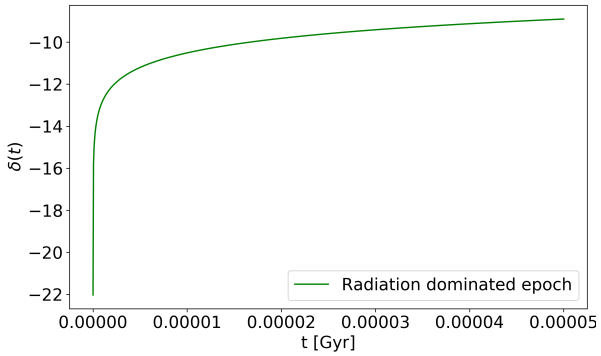

(a) *Radiation-epoch.*

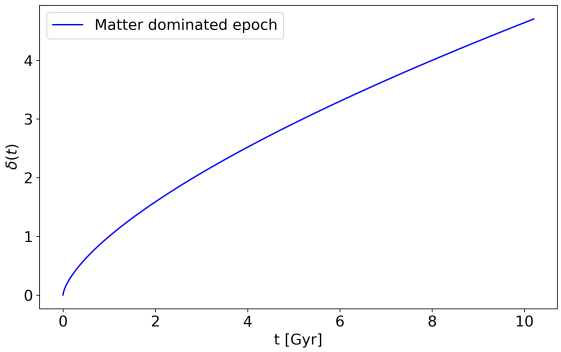

(b) *Matter-epoch.*

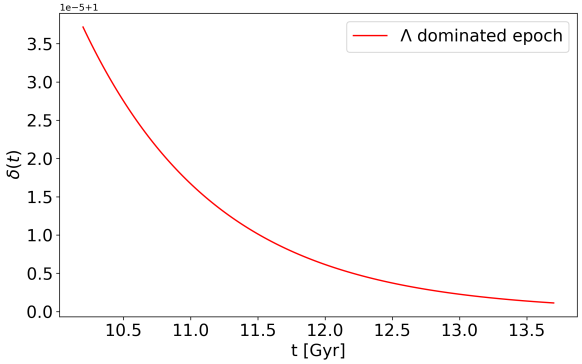

(c) Λ*-epoch.*

Figure 14: *Growth of density perturbations in matter in different epochs.*

In the matter dominated epoch, on the other hand, $\Omega_m = 1$ and $H = 2/(3t)$, which leads to the following version and solution of Equation (2.2.1),

$$\ddot{\delta} + 2\frac{2}{3t}\dot{\delta} - \frac{2}{3t}\delta = 0 \quad \Rightarrow \quad \delta(t) \approx D_1 t^{2/3} + D_2 t^{-1}, \tag{2.2.3}$$

where D_1 and D_2 depend on the initial conditions for $\delta(t)$. This solution has two modes, a decaying mode, t^{-1}, and a growing mode, $t^{2/3}$. Over time the decaying mode becomes negligible and the perturbations then grow at a rate of $t^{2/3}$, as can be seen in Figure 14b. It is in this epoch, that the density perturbations in matter grow significantly.

In the current epoch, which is dominated by the cosmological constant, $\Omega_m \ll 1$ once again. This time, however, $H = H_\Lambda$, leading Equation (2.2.1) to be,

$$\ddot{\delta} + 2H_\Lambda \dot{\delta} \approx 0 \quad \Rightarrow \quad \delta(t) \approx C_1 + C_2 e^{-2H_\Lambda t}, \tag{2.2.4}$$

where C_1 and C_2 depend on the initial conditions for $\delta(t)$. For this solution, the density perturbations grow as an exponentially decaying function, which can be seen in Figure 14c. As time goes by, the growth goes to zero, making structure formation stop.[37]

2.2.2 Our new model

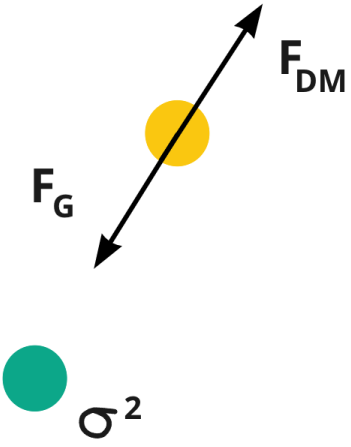

Figure 15: *A simple drawing of our proposed force.*

The purpose of this thesis is to test whether we in some way can predict the current acceleration through a new force generated by dark matter. As a reminder, we once again have a simple drawing of how the new, proposed force should work in Figure 15. The green and yellow dots are dark matter halos that attract each other through gravitational forces, F_G. When the dark matter particles within the green halo move, a velocity dispersion arises, σ^2, giving way for a new repulsive force, F_{DM}. In this scenario, we ignore the velocity of the halos due to the expansion of the Universe, in order to keep the model simple.

[37] Ryden 2017.

We are working on the basis of gravitational dynamics using Equation (2.1.2), which is given by,

$$\ddot{R}_m = -\frac{GM}{R^2}, \tag{2.2.5}$$

where G is the gravitational constant, M is the mass of the dark matter halos and R is the distance between the interacting dark matter halos. We can extend the gravitational acceleration by adding a term that depends on the squared velocity dispersion, σ^2, of the dark matter halos. We should then be able to see a change from the classic effects. The new, proposed acceleration becomes,

$$\ddot{R}_{DM} = \ddot{R}_m + \kappa \ddot{R}_\sigma, \tag{2.2.6}$$

where $\ddot{R}_m$ is the classic gravitational acceleration given by Equation (2.2.5), and $\ddot{R}_\sigma$ is the new term dependent on the squared velocity dispersion, σ^2, that we introduce. In order to make the new term comparable to the classic gravitational acceleration term, we multiply it with a dimensionless scaling factor, κ.

We propose that the new term dependent on the squared velocity dispersion, σ^2, can be given by,

$$\ddot{R}_\sigma = -\frac{GM}{R^2}\left(\frac{\sigma}{c}\right)^2, \tag{2.2.7}$$

where G, M and R are the same as before, σ is the velocity dispersion of the dark matter halos and c is the speed of light in vacuum, introduced to keep the equation in units consistent with an acceleration. We have chosen to make the expression for $\ddot{R}_\sigma$ very similar to the classic gravitational acceleration, $\ddot{R}_m$, in order to keep the model simple and easy to assess. Like the classic case, the mass is weighted linearly, such that heavier halos have a greater influence than the lighter halos. Since the heavier halos contain more dark matter particles, their velocity dispersion is also bigger than the velocity dispersions of the lighter halos, meaning that the force from the big halos should have a stronger effect.

Inserting Equation (2.2.5) and (2.2.7), we can rewrite Equation (2.2.6) as,

$$\ddot{R}_{DM} = -\frac{GM}{R^2}\left(1 - \kappa\left(\frac{\sigma}{c}\right)^2\right). \tag{2.2.8}$$

Like we did in Section 2.1.4, we can divide the acceleration generated by dark matter, $\ddot{R}_{DM}$, by the classic gravitational acceleration, $\ddot{R}_m$, to get the normalised acceleration.

$$\ddot{R}_{DM,norm} = \frac{\ddot{R}_{DM}}{\ddot{R}_m} = 1 + \kappa\frac{\ddot{R}_\sigma}{\ddot{R}_m}. \tag{2.2.9}$$

In order to determine the value of κ, we compare the normalised analytical acceleration given by Equation (2.1.33) and the normalised acceleration generated by dark matter, since these must be the same for the matter dominated epoch, $z > 0.6$, before the cosmological constant, Λ, starts to dominate the acceleration of the Universe.

$$\ddot{R}_{norm} = \ddot{R}_{DM,norm} = 1 + \kappa \frac{\ddot{R}_\sigma}{\ddot{R}_m} \Leftrightarrow \kappa = \frac{\ddot{R}_{norm} - 1}{\ddot{R}_\sigma / \ddot{R}_m}. \tag{2.2.10}$$

This leaves us with an expression for the scaling factor, κ, which allows us to compare the normalised analytical acceleration derived from the Friedmann equation and the normalised acceleration generated by dark matter. This makes it possible to test whether our model is applicable, as we will now explain.

Depending on the value of κ, the evolution of the acceleration of the Universe will look very different. In Figure 16 the normalised analytical acceleration for the Benchmark model (black) can be seen, along with our new model with three different κ-values (colored).

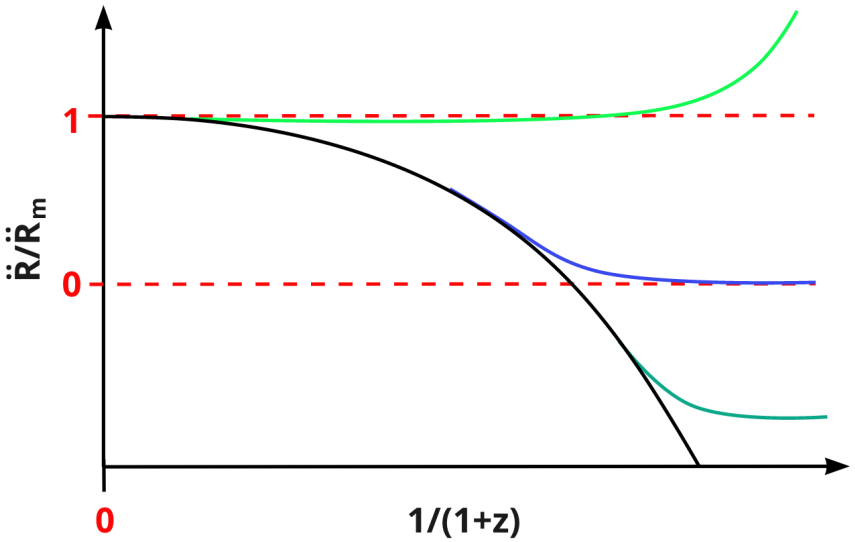

Figure 16: *The normalised analytical acceleration as a function of* $1/(1+z)$ *for the Benchmark model (black) and our new model with different* κ*-values (colored).*

The bright green line in the figure shows a model with a positive value of κ. If this was the case, we would see a deceleration of the Universe, instead of the

acceleration, that has been observed today through observations of supernovae and baryonic acoustic oscillations, as described in Section 1.1. From this, it is possible to conclude that the value of κ should be negative, which is the case for the blue and green curve, that both show the new model for an accelerating universe with two different κ-values. The greater the absolute value of κ is, the more time will pass before we start seeing a deviation from the Benchmark model, meaning that the green line has a larger absolute value of κ than the blue. As shown above in Equation (2.2.10), the value of κ is determined based on the two normalised accelerations, $\ddot{R}_{DM,norm}$ and $\ddot{R}_{norm}$, and is therefore not a value we choose.

2.3 Using RAMSES for creating simulations

If one wishes to explore the dynamics of the Universe at different times, it can be difficult to do so by using only analytical and empirical methods, since these have many limitations. A numerical simulation can be very convenient to overcome some of these constraints and this is a useful tool, since it gives us the opportunity to create a smaller, contained version of the real situation, that can be analysed and looked in-depth into. With numerical simulations we are able to look at structure formation at different times, which is needed for the purpose of our thesis. These simulations can be very complicated to create, since they have to be able to take into account complex formations and evolutions stemming from many different factors. However, these simulations also make it possible to simulate great periods of time and get otherwise unknown information on what the past or future either entailed or will entail.

In a numerical simulation of the Universe, initial conditions motivated by the Big Bang theory are generated and these are then evolved over time to get snapshots of a universe at different times. The idea behind this can be seen in Figure 17.

Dark matter N-body simulations are well tested, and since baryons are not included, the physics is simple. In these simulations, we have dark matter halos which are self-gravitating systems, where the system is held together by its own gravity. Furthermore cold dark matter is a collision-less fluid, which means that we can also look at the dark matter halos as collision-less systems. If baryons are included, the physics is more complex, since hydrodynamics now has to be added to the computations as well. Therefore it is simpler to look at a dark matter only simulation, and for the purpose of this thesis, baryons are not relevant, so we do not need to include these.[38]

[38]Martizzi 2019.

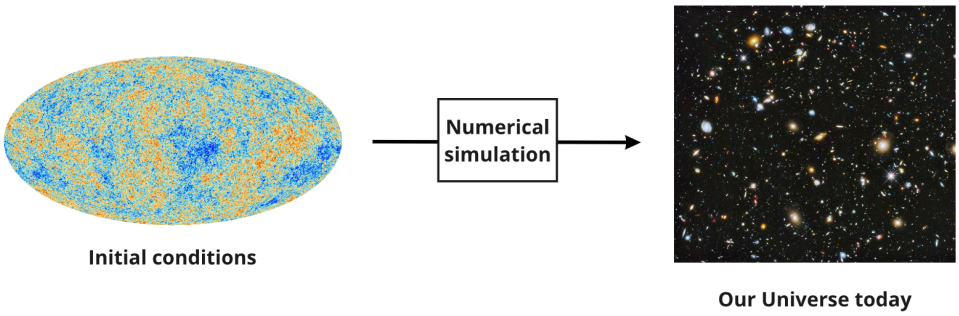

Figure 17: *The idea behind a numerical simulation where initial conditions are evolved to produce a snapshot of the Universe today. The CMB image is taken from*[39] *and the Hubble deep field image is taken from*[40].

In general, a code for N-body dynamics requires two different things. An algorithm to compute the force acting on each particle, and an algorithm to evolve particles forward in time. The initial conditions are created, where a certain amount of particles are put inside a box with given positions and velocities. Since the gravitational force in a given direction can be found by $\bar{F}(x) = -\nabla\Phi(x)$, the first algorithm calculates the gravitational force acting on each particle from all of the surrounding particles by solving Poisson's equation,

$$\nabla^2\Phi = 4\pi G\rho, \tag{2.3.1}$$

where Φ is the gravitational potential, G is the gravitational constant and ρ is the density. Once the code has calculated the gravitational force on each particle for a given time, we then know in which direction the acceleration will force the particle.[41]

The second algorithm is now applied, which uses a Kick-Drift-Kick (KDK) Leapfrog integrator to update the positions after a given time-interval. The workings of this can be seen in Figure 18.

[41] Martizzi 2019.

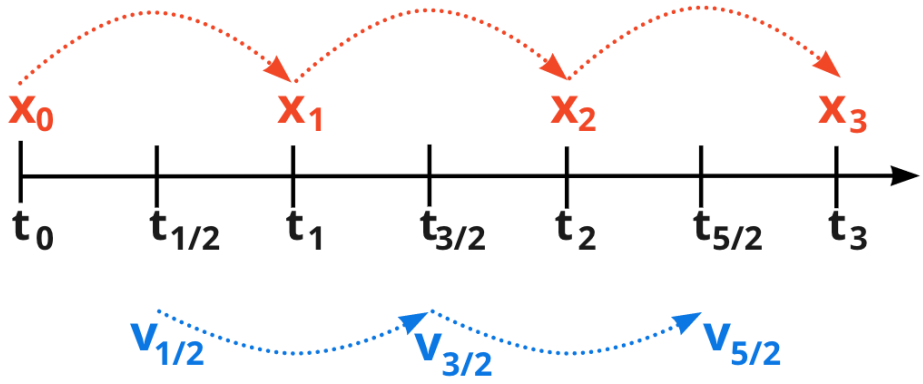

Figure 18: *An illustration of the KDK Leapfrog integrator.*

For a KDK Leapfrog integrator, the positions and velocities are updated back-to-back with a constant time interval. The positions are calculated for each time point, where the velocities instead are computed in between these, so at the mid-points of the time intervals. This means that while the positions of the particles are being updated, the velocities, needed to find the next positions, are being computed, creating this continuous cycle of parallel calculations. The advantages of using a KDK Leapfrog integrator is that it is simple and time reversible, which warrants the conservation of energy and angular momentum. This means, that if we backstep the process, the results of previous steps will still be exactly the same.[42]

In our thesis, we have used numerical simulations produced with The RAMSES project[43], which provides snapshots of the structure of the Universe at given redshifts. RAMSES is a Fortran written code, which uses Adaptive Mesh Refinement, AMR. This means, that instead of using a pre-determined locked grid, the code allows for the grid to have different levels of refinement depending on the needed resolution for each area. An illustration of this can be seen in Figure 19.

[42]Dehnen, W. and Read, J. I. 2011.
[43]Teyssier 2002.

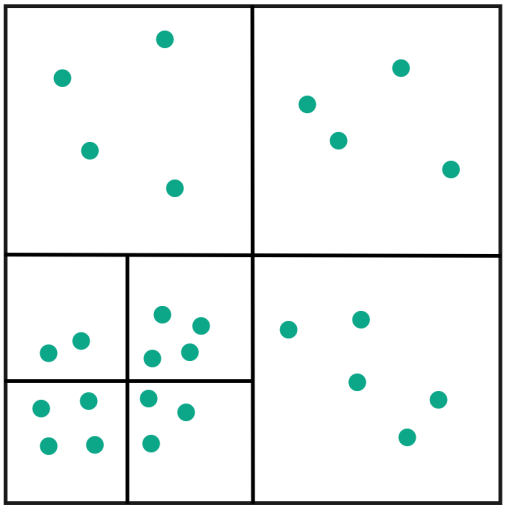

Figure 19: *An illustration of Adaptive Mesh Refinement, AMR.*

With AMR we are able to achieve a high resolution where needed, without expensive computational time, since the finer mesh is only applied to the areas of interest. If we wanted a high resolution in the case of the pre-determined grid, we would have to apply this fine mesh to the entire simulation wasting a lot of time computing a high resolution of empty regions.[44]

RAMSES takes in initial conditions describing the kind of universe we are working with and can then evolve these conditions to show us the evolution of this universe. The initial conditions have been produced using MUSIC (MUlti-Scale Initial Conditions)[45], which creates a statistical representation of a universe with given cosmological parameters. In our case, it takes starting conditions equivalent to the Universe at the time of CMB emission and propagates these linearly until the desired redshift has been reached. With this, the initial conditions have been produced and the simulation can then start.[46]

By using MUSIC, we can adjust the number of particles in the simulation, N, by choosing a level, l, which is related to the number of particles through $N = (2^l)^3$. The number of particles in a simulation can be seen in Table 1 for different levels. Among other things, we can also adjust the the final size of the simulated

[44]Berger, M. J. and Colella, P. 1989.
[45]Hahn, O. and Abel, T. 2011.
[46]Binney, J. and Tremaine, S. 2008.

universe, `boxlength`, the redshift the simulation starts at, `zstart`, and the density parameters of the different components in the Universe today, `Omega_m` and `Omega_L`.

Level, l	Number of particles, N
6	262144
7	2097152
8	16777216
9	134217728

Table 1: *A given level, l, and the related number of particles, N, in a simulation.*

3 Method

In this section, we describe our simulation and the parameters used when generating this. We explain how we intend to test and analyse our simulation in order to see whether our model can predict the acceleration of the Universe.

3.1 Acceleration of the Universe

In order to see if our model can describe what we see in the Universe today, we need to know how the Universe evolves over time. We do this, by calculating the normalised analytical acceleration of the Universe using Equation (2.1.33), which is derived from the Friedmann equation,

$$\ddot{R}_{norm} = 1 + 2\frac{\Omega_{r,0}}{\Omega_{m,0}} r^1 R^{-1} - 2\frac{\Omega_{\Lambda,0}}{\Omega_{m,0}} r^{-3} R^3,$$

where R is the radius of the sphere we looked at, in physical units, when deriving the Friedmann equation, shown in Figure 10 in Section 2.1.1, and r is the comoving radius of the sphere. Since the radius, R, depends on the scale factor, a, through $R = a \cdot r$, and the scale factor is related to the redshift through $a = 1/(1+z)$, we can look at how the acceleration evolves as a function of redshift. In Table 2, the values of the different parameters used in the acceleration equation can be seen. These are all corresponding with the Benchmark model.

Parameter	Value
$\Omega_{m,0}$	0.3089
$\Omega_{\Lambda,0}$	0.6911
$\Omega_{r,0}$	$9 \cdot 10^{-5}$
H_0	$2.1951 \cdot 10^{-18}$ s^{-1}
r	5 Mpc

Table 2: *Values of the different parameters used in Equation (2.1.33).*

3.2 Our Simulation

In our thesis we are interested in looking into a possible scenario that can explain the already observed workings of the Universe, without the cosmological constant, through numerical simulations. However, we still need for the effect of dark energy to be a part of the simulation and therefore we keep the Λ-component when generating it, by letting $\Omega_\Lambda = 0.69$. We have created a simulation using RAMSES with $2.1 \cdot 10^6$ particles, which is equivalent to level $l = 7$. This simulation does

not contain any baryons and consists only of dark matter, since we are interested in exploring the effects of this. In Figure 20 snapshots of our simulation at three different redshifts can be seen. Here it is possible to see the evolution of structures and the large scale structure.

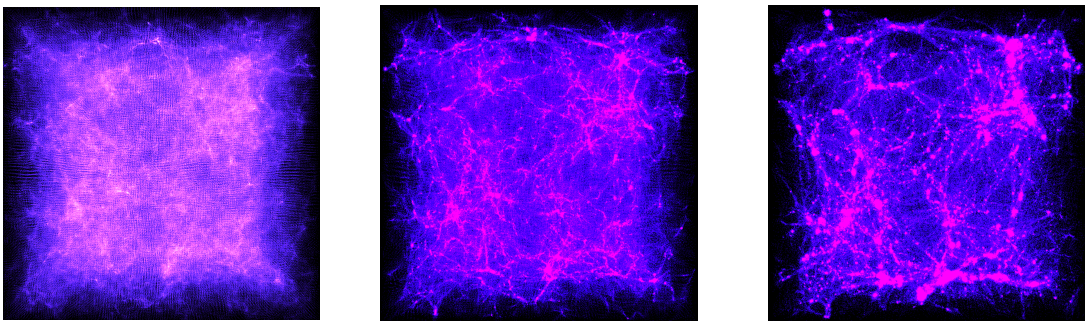

(a) *Snapshot at* $z = 5.20$. (b) *Snapshot at* $z = 1.77$. (c) *Snapshot at* $z = 0.02$.

Figure 20: *Snapshots of our simulation at three different redshifts.*

The initial conditions for the simulation have been produced using MUSIC and can be seen in Table 3. Since the density of the Universe is known, the mass of the dark matter particles varies, depending on the volume and number of particles that is chosen. For our simulation, the particle mass is $1.6 \cdot 10^{10}$ kg.

Parameter	Value
`boxlength`	96 Mpc
`zstart`	20
`Omega_m`	0.3089
`Omega_L`	0.6911
`H0`	67.74

Table 3: *Initial conditions for our simulation.*

3.2.1 Testing the Friedmann equation

Once the outputs containing the snapshots of the simulation at different redshifts have been given, we are able to examine the laws of physics and the evolution of the Universe. To do this, we make sure that the Friedmann equation behaves as expected in our simulated universe. In the matter dominated epoch, only matter influences the acceleration of the Universe, making the acceleration of the Universe equal to the gravitational acceleration. We can calculate the gravitational acceleration felt by the dark matter particles in our simulation, and compare this

to the acceleration of the Universe in the matter dominated epoch, which is given by Equation (2.1.32),

$$\ddot{R}_{m,analytical} = -\frac{H_0^2}{2}\Omega_{m,0} r^3 R^{-2}.$$

In order to calculate the gravitational acceleration, we find the acceleration that would be felt by a dark matter particle, on the edge of a sphere with a given radius, by all other particles located within the sphere, which can be seen in Figure 21. To do this, we use Equation (2.2.5), which is the classic equation for the gravitational acceleration and in this case is given by,

$$\ddot{R}_m = \sum_i -\frac{GM_i}{R_i^2}, \tag{3.2.1}$$

where G is still the gravitational constant, M_i is the mass of the particles within the sphere and R_i is the distance in physical units from the particle on the edge to a given particle within the sphere. Since we have a simulation of two million particles, it would be very time consuming to find the acceleration through this method for each particle, so instead, we select a certain number of particles to use and then create an average based on what these chosen particles feel.

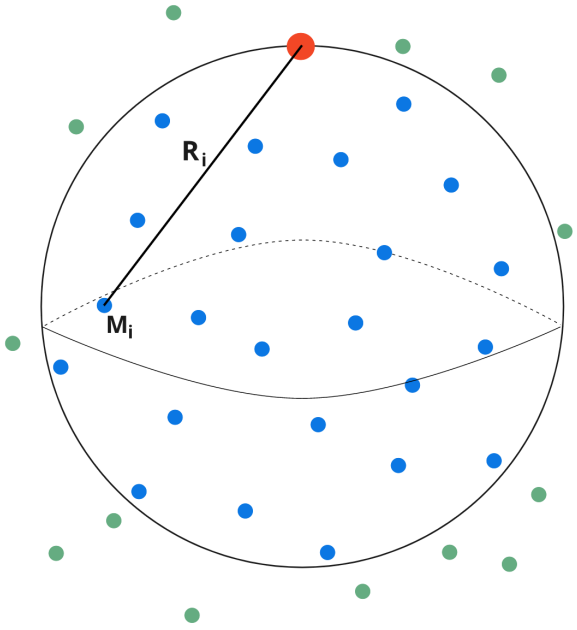

Figure 21: *An illustration of a particle on the edge of the sphere (red) and the particles within the sphere (blue) with mass, M_i, and distance to the particle on the edge, R_i. Particles outside the sphere are colored green.*

Our simulated universe, unlike the actual universe, has a finite size and a square shape, so we apply a grid of $5 \times 5 \times 5$, meaning that we now have 125 grid points to describe our simulation by. This is illustrated in Figure 22, where one of the grid points have been circled. These grid points are used for deciding which particles to use for our calculations.

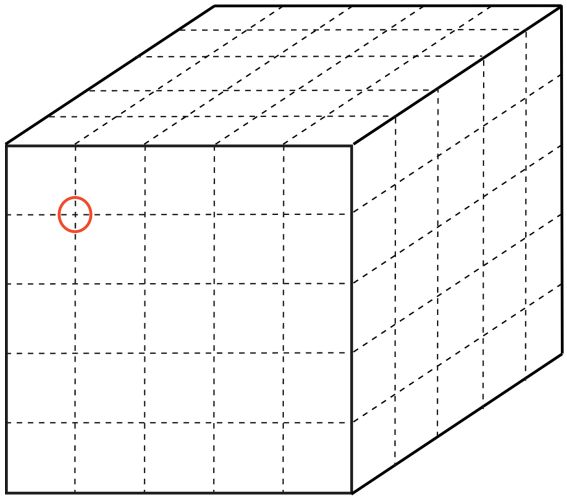

Figure 22: *An illustration of the* $5\times5\times5$ *grid applied to the numerical simulation, where one of the grid points have been circled.*

Since we are interested in calculating the acceleration felt from a particle on the edge of a sphere, we need the particle to be in an area, where there are enough particles to draw a complete sphere around. The particles at the outer grid points are limited by the ends of the simulation and are therefore dismissed, since our simulation has periodic boundary conditions, PBCs. PBCs are used for simulating infinite systems, by creating one small, representative system and then using this system as its own neighbor on all sides[47], as can be seen in Figure 23. Here, the green square in the middle is our simulation box and the surrounding white squares are copies of this universe. If we look at particle A, we see that it has a neighbor outside of the simulation box, particle B. Due to the PBCs, particle B is exactly the same particle as the one that is located on the opposite side of the simulation box from particle A. If we were to draw a sphere with particle A on the edge, this sphere would go outside of the simulation box and include particle B, which

[47]Kuzkin 2014.

actually belongs to the other side of the simulated box.

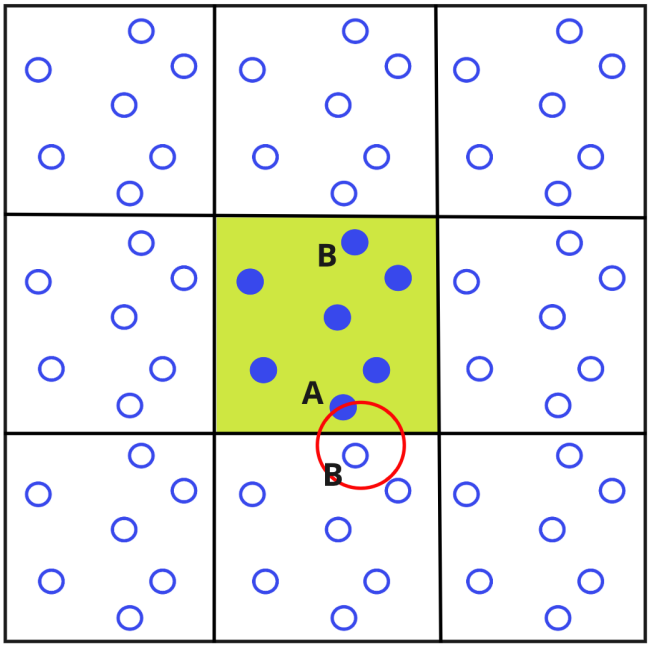

Figure 23: *A simple figure of periodic boundary conditions, PBCs.*

Once we have dismissed the 61 outer gridpoints due to the PBCs, we are left with 64 inner grid points to use. Here, we locate the nearest particle to the grid point and put this at the edge of a sphere with a radius of $r = 5$ Mpc in comoving coordinates. We then calculate the acceleration that the particle at the edge of the sphere feels from each of the particles within the sphere. We continue to do this for all of the particles located at the grid points and then find an average of these.

Since the simulation is supposed to be a description of our Universe, the 3D box that is our simulation is expanding, ending with a boxsize of 96 Mpc, as stated in Table 3. All of the coordinate dependent values that are given from the simulation are given in terms of code lengths, which describe their location compared to the relative size of the box at the given snapshot. In order to prevent confusion, all of the values are converted from code lengths to physical units by multiplying the values with a length unit, L, which is the boxsize at the given snapshot in physical coordinates,

$$x_{physical} = x_{codelength} \cdot L = x_{codelength} \cdot \texttt{boxsize} \cdot \left(\frac{1}{1+z}\right) \tag{3.2.2}$$

3.2.2 Analysing the simulation

We wish to identify structures, such as dark matter halos in our simulation. For this, we use the HOP Halofinder in The yt Project[48]. In Figure 24 an illustration of the HOP Halofinder can be seen, where each dot corresponds to a particle. This method works by calculating the local density of each particle and then for each particle locating its densest neighbor with a higher density than itself. These are then connected, which is illustrated through the dotted lines. The code continues by looking for the densest neighbor of this new particle and continues on until a particle is its own densest neighbor, meaning that the surrounding particles all have lower densities. When this has been found, all of the previous particles are connected to this in a chain, with the densest particle (the filled dots in the figure) as the end link of the chain. The chains with the same end links are then connected to form a halo, which is illustrated by the particles having the same color.[49]

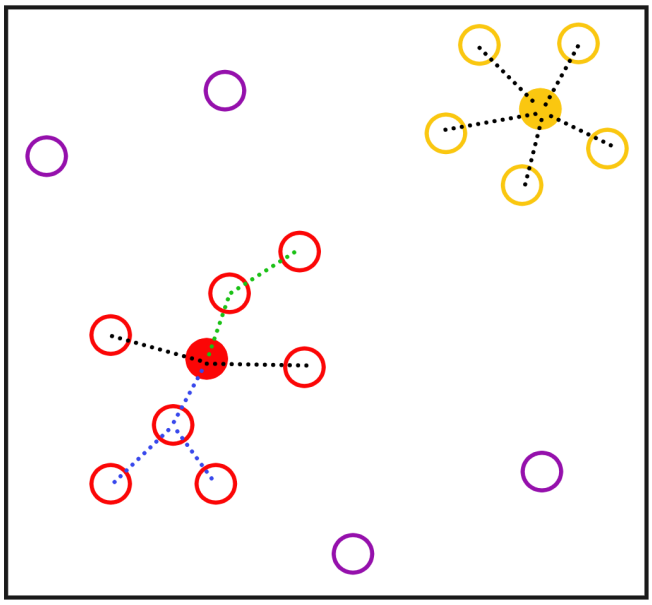

Figure 24: *A simple illustration of the HOP Halofinder method.*

From the HOP Halofinder, we find that the amount of halos in the simulation increase from 10 to 1600, as the redshift decreases and we get closer to today. From the Halofinder we are also given the values of the halos, that we need for our

[48]Turk et al. 2010.
[49]Eisenstein, D. J. and Hut, P. 1998.

analysis, such as velocity dispersions, σ, masses, M, virial radii and coordinates for all halos.[50]

By looking at the number of particles in our halos, found from the Halofinder, we conclude that the halos only contain about 1/3 of the total particles of our simulation. The rest of these particles are instead part of smaller structures that are not big enough for the HOP Halofinder to identify them as halos or else they lie in the void between the structures. It is therefore necessary to also evaluate whether there might be smaller sub-structures, that need to be included when we want to analyse our simulation further. In order to check this, we locate all particles not part of a halo and find the ones with the deepest mass potentials.

In order to find the possible structure surrounding a deep potential particle, we analyse the neighborhood of the given particle. We know from the halos found using the Halofinder that the average density of a halo is $\rho_{halo} = 8.0 \cdot 10^{-25}$ kgm^{-3}. By dividing this value by the he critical density of the Universe, $\rho_{c,0} = 8.7 \cdot 10^{-27}$ kgm^{-3} [51], we are able to find the typical density within a virial radius of the center of the halos,

$$\frac{\rho_{halo}}{\rho_{c,0}} = \frac{8.0 \cdot 10^{-25}\,\mathrm{kgm}^{-3}}{8.7 \cdot 10^{-27}\,\mathrm{kgm}^{-3}} = 92.7. \tag{3.2.3}$$

From this we find that the virial radius for the substructure surrounding the particles needs to have a density of 93 ± 10 times the critical density, to include structures close to this density. To avoid the substructures becoming too large, we put in a maximum size of the virial radius. If we did not have an upper limit for the virial radius, the code would just keep increasing the radius in order to find a density within the virial radius big enough for the wanted relationship. If the maximum size of the virial radius is surpassed, the particle is dismissed.

We found at most about 20 substructures for low redshifts and no structures at all for the higher redshifts, which means that compared to the numerous amount of structures found using the Halofinder, these are rather insignificant on the big scale and can be dismissed entirely.

3.2.3 Our new model

Now that we have located the dark matter halos in our simulation, we can use these for testing whether we can predict the acceleration of the Universe through a new acceleration generated by dark matter. We use the same procedure as applied

[50] *Halo Finding and Analysis* n.d.
[51] Ryden 2017.

in Section 3.2.1, but instead of looking at the acceleration felt by the individual particles, we consider the acceleration felt by the dark matter halos.

We create an average acceleration based on the halos selected by applying a $5\times5\times5$ grid again. Due to the periodic boundary conditions, we find the halos located close to the 64 inner grid points. Each of these halos are put at the edge of a sphere, as it can be seen in Figure 25, and the acceleration that one halo (cyan) feels from all halos within the sphere (purple) is then calculated. We want the spheres to have a radius of $r = 9.8$ Mpc in comoving coordinates, in order to prevent the spheres from overlapping and including the same halos twice.

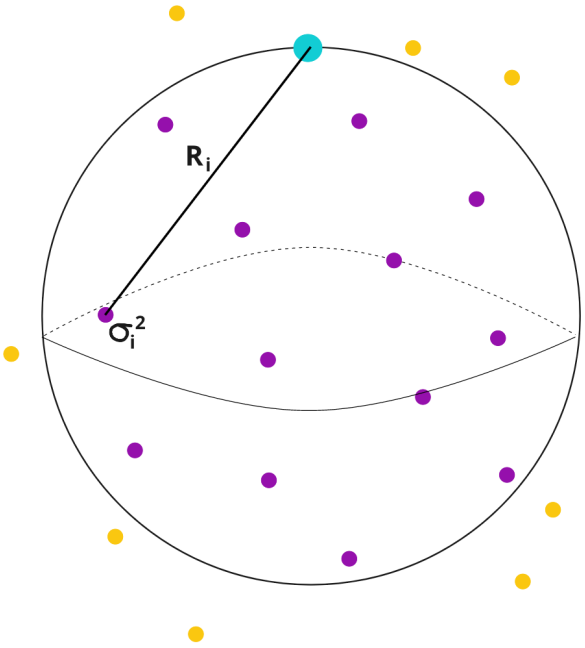

Figure 25: *An illustration of a halo on the edge of the sphere (cyan) and the halos within the sphere (purple) with velocity dispersion, σ_i, and distance to the halo on the edge, R_i. Halos outside the sphere are colored orange.*

In Section 2.2 we introduced a new acceleration that arises when two dark matter halos interact with each other, due to the velocity dispersion of one halo. Since we are now looking at a scenario where we have an interaction of several dark matter halos, we want to find the acceleration that the halo on the edge of the sphere feels from the force created by the velocity dispersions of all of the halos within. By

adding a summation symbol to Equation (2.2.8), we find the following formula,

$$\ddot{R}_{DM} = \sum_i -\frac{GM_i}{R_i^2}\left(1 - \kappa\left(\frac{\sigma_i}{c}\right)^2\right), \tag{3.2.4}$$

where M_i is the mass of the halos within the sphere, R_i is the distance in physical units from the halo on the edge to a given halo within the sphere and σ_i is the velocity dispersion of the halos within the sphere. This equation describes our new model that we wish to explore using our simulation. This will be used in Section 4.3.

4 Results

In this section, we start off by making sure that our simulation agrees with the Benchmark model and verify that our simulation is a reliable representation of the Universe. We then present the results of the analysis of our model, along with the results of an extension of the model. This is done in order to have different variations of our model, in case one might be a better fit than the others.

4.1 Acceleration of the Universe

We are interested in comparing our model to the Universe we observe today. In order to make this an easier task, we compare our new model to the normalised analytical acceleration of the Universe, given by the Benchmark model. In Figure 26 the normalised analytical acceleration as a function of $1/(1+z)$, is shown in order to see how this evolves over time. This acceleration is given by Equation (2.1.33),

$$\ddot{R}_{norm} = \frac{\ddot{R}}{\ddot{R}_{m,analytical}} = 1 + 2\frac{\Omega_{r,0}}{\Omega_{m,0}} r^1 R^{-1} - 2\frac{\Omega_{\Lambda,0}}{\Omega_{m,0}} r^{-3} R^3.$$

The values for this equation can be seen in Table 2.

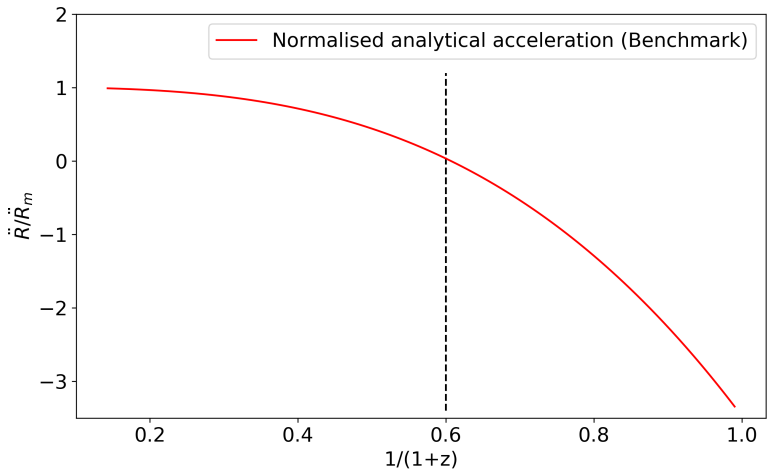

Figure 26: *The normalised analytical acceleration of the Universe as a function of* $1/(1+z)$ *given by the Benchmark model.*

The dashed line in Figure 26 indicates the beginning of the Λ dominated epoch at $1/(1+z) \simeq 0.6$, which means that the matter dominated epoch is on the left-hand

side of the dashed line, and the Λ dominated epoch is on the right-hand side of the line. In the matter dominated epoch the normalised acceleration is 1 in the beginning, since matter only influences the acceleration, but in the Λ dominated epoch the cosmological constant takes over and the normalised acceleration drops dramatically.

If we take a closer look at the matter dominated epoch in the left-hand side of Figure 26, we can verify that our simulation agrees with the Friedmann equation and the Benchmark model for this epoch. Following Section 3.2.1, we calculate the gravitational acceleration that applies in our simulation in this period, which can be seen as the numerical acceleration (blue) in Figure 27.

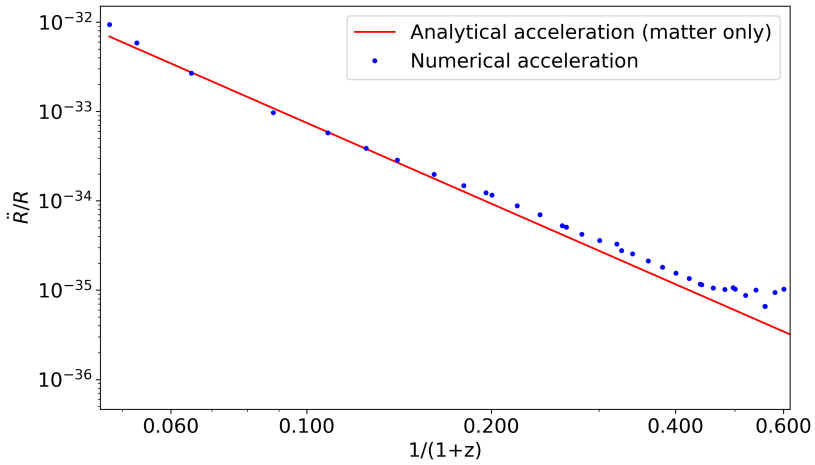

Figure 27: *The numerical acceleration for our simulation (blue) and the analytical acceleration as a function of* $1/(1+z)$ *for the Benchmark model (red).*

Here we have chosen to plot $\ddot{R}/R$ on a loglog scale as a function of $1/(1+z)$, since this gives us a straight line. It is therefore easier to compare the gravitational acceleration calculated from our simulation and the analytical acceleration corresponding to the Benchmark model in the matter dominated epoch. We see that the numerical acceleration (blue) fits well with the analytical acceleration (red), which means that our simulation is consistent with the Benchmark model. Towards the end, we see the numerical acceleration starting to deviate from the predicted model. This happens, as we approach the epoch where the cosmological constant starts dominating, which forces the acceleration of the universe to diverge from the evolution of the matter dominated epoch.

4.2 Verifying our simulation

We have just shown that our simulation agrees with the Benchmark model for the matter dominated epoch, however we want to explore how reliable this simulation actually is and whether this is a good representation of the Universe. One way of doing this, is by looking at the distribution of halos according to their masses. In Figure 28, a theoretical model of a halo mass function can be seen for redshift, $z = 0$, where the masses range from 10^8 $M_\odot$ to 10^{16} $M_\odot$. A halo mass function describes the number density of dark matter halos for the mass range.[52]

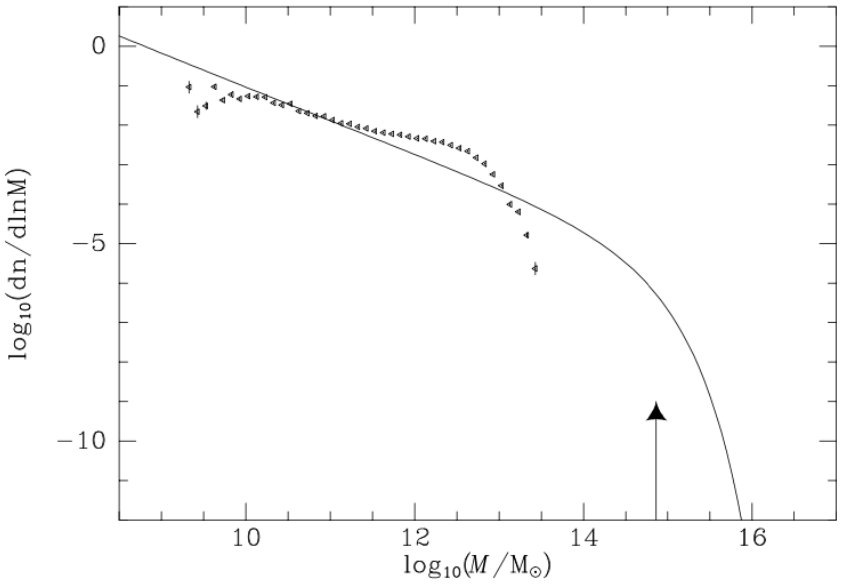

Figure 28: *The mass function of halos in the standard ΛCDM model for redshift, $z = 0$ (solid line). The symbols show a galaxy luminosity function, which is not relevant in our thesis.*[53]

From this figure we see that we have a great number of small halos and that the number of halos falls quickly as the masses of the halos increase. This agrees with the nature of structure formation, since the creation of the smaller structures only take a short while compared to the bigger structures that are just now being created today.[54] In Figure 29 the halo mass distribution can be seen for our simulation as a comparison to the theoretical graph in Figure 28. However, instead of plotting a halo mass function, we have chosen to just plot a distribution showing the number

[52]Binney, J. and Tremaine, S. 2008.
[54]Baugh 2006.

of halos as a function of mass. This is done in order to get a simple and intuitive understanding of the distribution of halos, since the halo mass function requires complicated calculations.

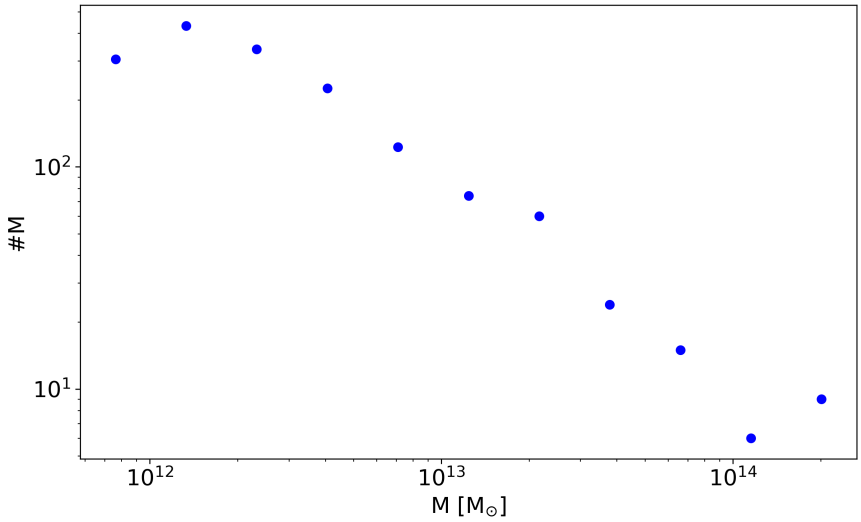

Figure 29: *The halo mass distribution of our simulation for redshift,* $z = 0.02$.

This halo distribution has been found by binning the halo masses of our simulation for our latest redshift at $z = 0.02$. We see that our distribution spans a much smaller mass range, but overall follows the same characteristics of the halo mass function in Figure 28, where we see an abundance of smaller mass structures.

When looking at the tails of the halo mass distribution in Figure 29, we see that there are some fluctuations, which makes our simulation uncertain for masses lower than 10^{12} $M_\odot$ and higher than 10^{14} $M_\odot$. Due to this, our reliable mass range is only a small fraction of the theoretical range, that spans from 10^8 $M_\odot$ to 10^{16} $M_\odot$. As explained in Section 3.2.2, our halos only contain 1/3 of the total number of particles of our simulation, meaning that the smaller halos, that might make up for the masses lower than 10^{12} $M_\odot$, are lost.

4.2.1 Creating additional simulations

In order to improve our limited mass range, we create two new simulations. These are produced in the same way that our original simulation has been created, with

the same cosmological parameters that were shown in Table 3. These new simulations contain a larger amount of particles, where the volume has been kept intact for one simulation and has been increased for the other. To easily distinguish between them, we will refer to them as Universe A, B and C, where Universe A is our original simulation. Universe B and C are the two new simulations and their parameters can be seen in Table 4.

	Uni A	Uni B	Uni C
Level	7	8	8
N	$2.1 \cdot 10^6$	$16.8 \cdot 10^6$	$16.8 \cdot 10^6$
`boxlength`	96 Mpc	96 Mpc	191 Mpc
Particle mass	$1.6 \cdot 10^{10}$	$2.1 \cdot 10^9$	$1.6 \cdot 10^{10}$

Table 4: *The size, number of particles and particle mass for our three different simulations.*

For Universe B, we have kept the size of the box and thereby the volume of the simulated universe the same as for our original simulation, Universe A. Instead, we have increased the number of particles by a factor of eight, in order to see how this combination affects the resolution of the simulation. Both the amount of particles and the boxsize has been multiplied by eight in Universe C, making this simulation similar to Universe A. Since the density of the Universe is known and kept intact in our simulations, the mass of the dark matter particles in Universe B is smaller than Universe A and C.

With these new simulations, we can once again produce a graph showing the halo mass distribution for Universe A, B and C, in order to see if our mass range has been improved by creating these additional simulations. The halo mass distribution for all three simulations can be seen in Figure 30.

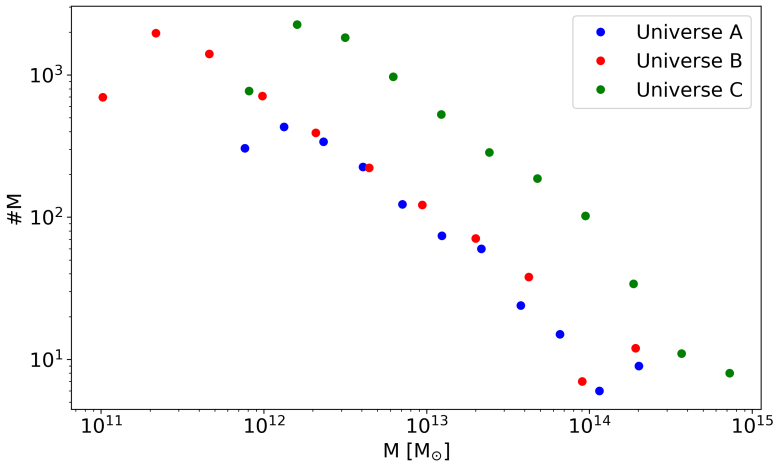

Figure 30: *The halo mass distribution of our three universes.*

The figure shows that Universe A and Universe C follows the same shape, but since Universe C contains eight times the number of particles as Universe A, the distribution is shifted upwards by a factor of eight. Universe B contains a larger amount of small structures than Universe A and C, because it contains more particles on a smaller volume, giving it a much better resolution on small scales. This happens since the particle mass is smaller for Universe B, compared to the other two universes, such that the particles take longer to congregate.

Universe A and Universe B are both affected by their small volumes, which means that they become uncertain when looking at masses higher than 10^{14} $M_\odot$. Since Universe C has a larger volume, it is more accurate at higher masses, such that we can evaluate masses up to 10^{15} $M_\odot$. At lower masses, on the other hand, Universe C along with Universe A start to become inaccurate. For these two simulations, the masses below 10^{12} $M_\odot$ are unreliable. For these low masses, we can instead look at Universe B, where we can look at masses close to 10^{11} $M_\odot$. From this we see, that by creating these two additional simulations, we have increased our original mass range from 10^{12} $M_\odot$ to 10^{14} $M_\odot$ and can now consider halos ranging from 10^{11} $M_\odot$ to 10^{15} $M_\odot$.

However, this range is still far from the theoretical mass range of 10^8 $M_\odot$ to 10^{16} $M_\odot$ in Figure 28. We are therefore interested in finding out if this will affect the analysis of our new model. Our proposed acceleration generated by dark matter depends on the velocity dispersion of dark matter halos and we can therefore look

at the correlation between the mass and the velocity dispersion of these halos. In Figure 31 this relation can be seen for each of the three universes at their latest redshifts.

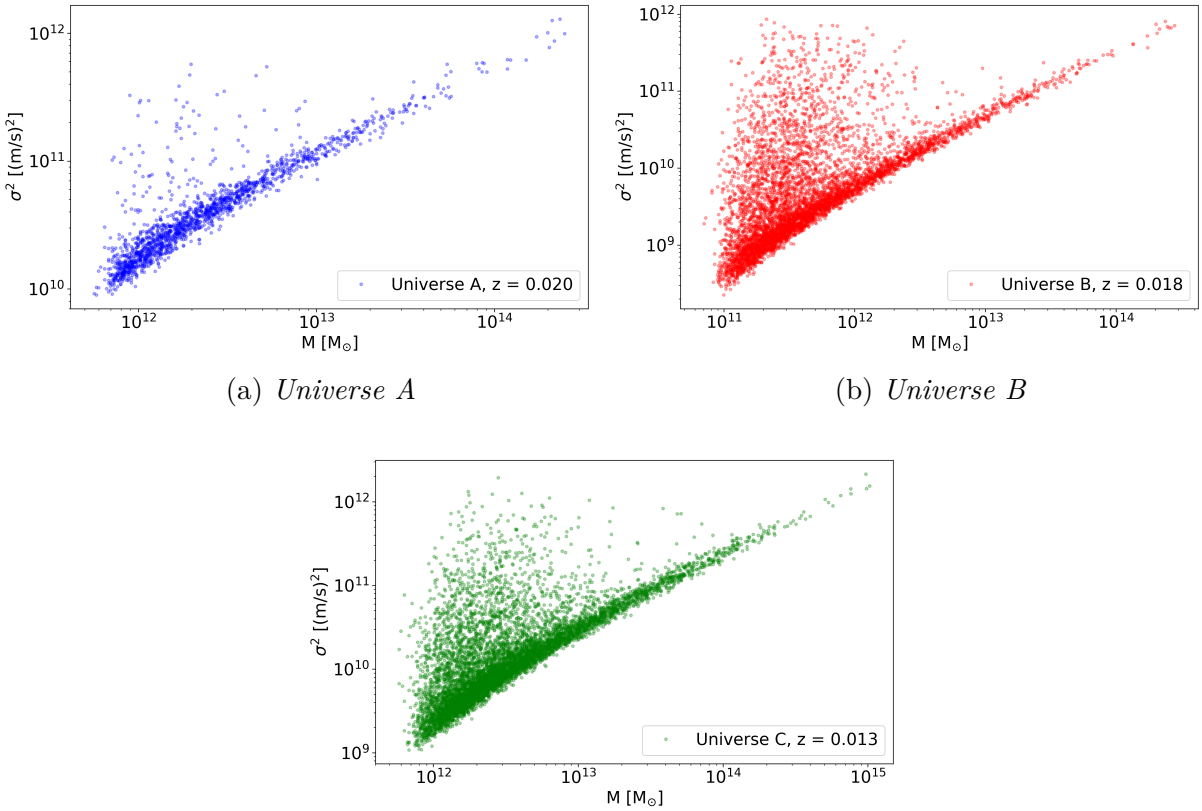

(a) *Universe A* (b) *Universe B*

(c) *Universe C*

Figure 31: *The velocity dispersion of dark matter halos, σ^2, as a function of halo masses for our three universes at their latests redshifts.*

In the figure, we see a clear correlation where the small halos likewise have small velocity dispersions and the big halos have correspondingly big velocity dispersions. Most halos follow this correlation, though some of the smaller halos have greater velocity dispersions, than would be expected, due to the halos not yet being in dynamic equilibrium. From the halo mass distribution in Figure 30, we saw that we have an abundance of smaller structures, but since their velocity dispersions are equivalently small, their impact on the acceleration generated by dark matter is negligible. This means, that even though we are missing structures with masses less than 10^{11} $M_\odot$, we will not see a significant difference. We should expect

to see a great impact of the bigger halos, due to their big velocity dispersions, however since these are so few in numbers, we will not see a noticeable change when excluding the halos with masses larger than 10^{15} $M_\odot$.

A remaining concern might be the accuracy of our simulations and their ability to describe our Universe. To account for statistical fluctuations, we have created four extra simulations for each of the three universes. These new simulations are created with the same parameters as Universe A, B and C, respectively, but each have different random seeds that create specific initial conditions for each simulation. This gives us 15 simulations in total; five simulations of Universe A, five simulations of Universe B and five simulations of Universe C.

To check that the simulations are in agreement with each other and thereby can be used to make our future results more accurate, we have once again plotted the halo mass distribution. This can be seen in Figure 32, where all five simulations of Universe A can be seen as the blue data points, the five simulations of Universe B are the red data points and the green data points show the five simulations of Universe C. From this figure we see that all simulations of each universe are consistent with each other.

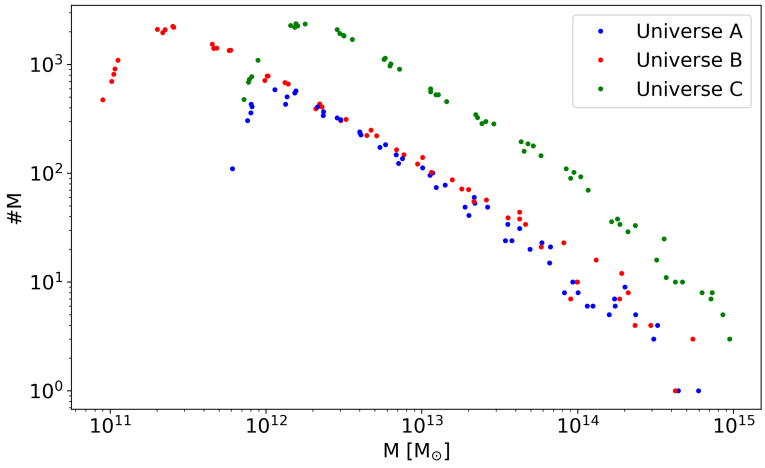

Figure 32: *The halo mass distribution of all five simulations for each of the three universes.*

4.3 The effects of our new model

Now that we have created additional simulations and tested them, we know that we are able to use them as a reliable sample of our Universe. This makes it possible for us to use them for testing the theory of our new model. We want to see whether it is possible for us to predict the acceleration of the Universe, through the movement of dark matter particles.

Figure 33 shows the normalised acceleration, $\ddot{R}_{DM,norm}$ generated by dark matter for the three universes, given by Equation (2.2.9),

$$\ddot{R}_{DM,norm} = \frac{\ddot{R}_{DM}}{\ddot{R}_m},$$

where $\ddot{R}_{DM}$ and $\ddot{R}_m$ are given by Equation (3.2.4) and Equation (3.2.1) respectively,

$$\ddot{R}_{DM} = \sum_i -\frac{GM_i}{R_i^2}\left(1 - \kappa\left(\frac{\sigma_i}{c}\right)^2\right), \quad \ddot{R}_m = \sum_i -\frac{GM_i}{R_i^2}.$$

We have chosen to show only one of the five simulations for each universe in Figure 33, since the simulations for each are very similar.

Figure 33a, 33b and 33c show our numerical model for the normalised acceleration generated by dark matter for Universe A, B and C respectively (blue) along with the analytical acceleration for the Benchmark model (black). The bold data points and their errorbars represent the mean value of each of five bins that the data points have been divided into. This will be explained in the following section.

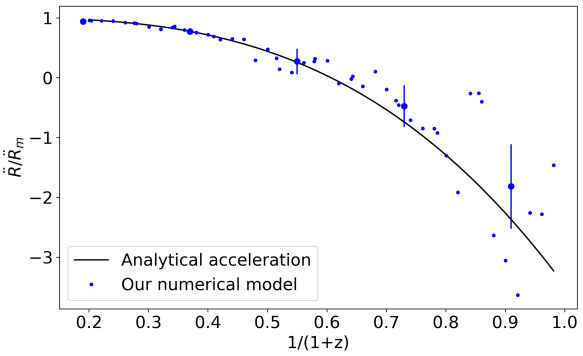

(a) *Universe A, Simulation 3.*

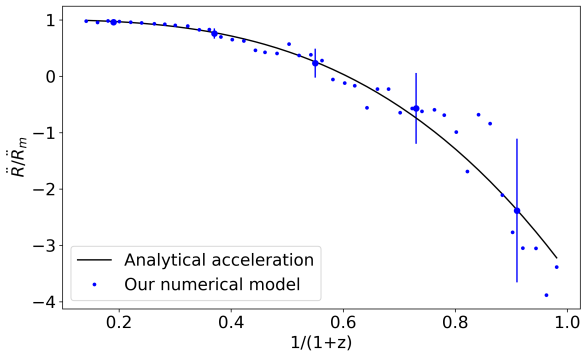

(b) *Universe B, Simulation 2.*

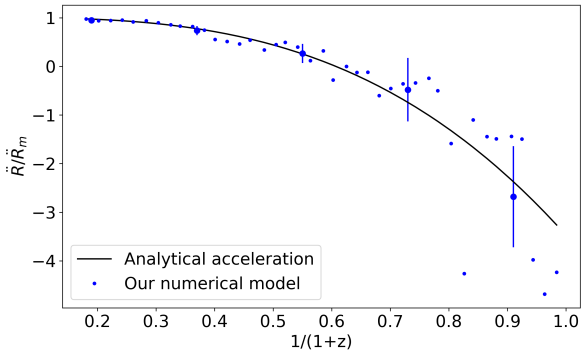

(c) *Universe C, Simulation 4.*

Figure 33: *Our numerical model for the normalised acceleration generated by dark matter of our three universes (blue) and the normalised analytical acceleration for the Benchmark model (black).*

The data points in Figure 33 seem to follow the tendency of the analytical curve well, and we see that every mean value fits the analytical model with its errorbar. We do however see, that Universe A and C have a few outliers. This could be due to the fact that Universe A contains eight times fewer particles than the other universes, which makes it a less accurate model of our actual Universe. Universe B and Universe C contain the same number of particles, but Universe C has an eight times larger volume than Universe B, which gives it the same configuration as Universe A. From looking at Figure 33b, we see that the normalised acceleration generated by dark matter in Universe B follows the normalised analytical acceleration with almost no outliers. This could be a consequence of Universe B containing a large amount of particles in a small volume.

To confirm that our limited mass range is sufficient in the evaluation of our model, we have examined our model for Universe B for masses higher than 10^{12} $M_\odot$, since this is the only simulation that contains masses lower than 10^{12} $M_\odot$. This can be seen in Figure 34a. Similarly, we have looked at our model for Universe C for masses lower than 10^{14} $M_\odot$, since this simulation is the only simulation of the three with masses higher than 10^{14} $M_\odot$. This is shown in Figure 34b.

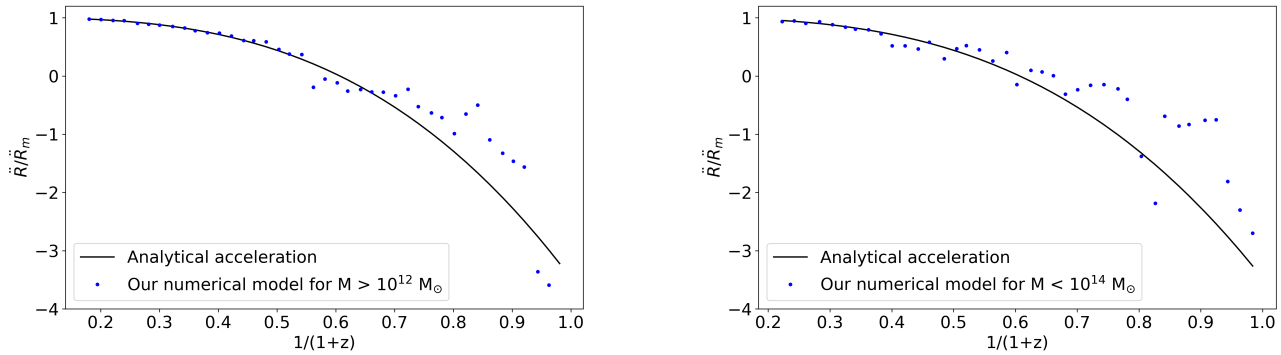

(a) *Universe B for* $M > 10^{12}$ $M_\odot$. (b) *Universe C for* $M < 10^{14}$ $M_\odot$.

Figure 34: *Our numerical model for the normalised acceleration generated by dark matter of our three universes (blue) and the normalised analytical acceleration for the Benchmark model (black).*

From Figure 34 we that there is no apparent difference between these altered graphs, compared to the entirety of them in Figure 33b and 33c. This means that our mass interval is a reliable sample range.

The κ-values have been calculated with Equation (2.2.10),

$$\kappa = \frac{\ddot{R}_{norm} - 1}{\ddot{R}_\sigma / \ddot{R}_m},$$

for $z > 0.6$, since we want to make sure that our data points fit the normalised analytical acceleration in this region. These values can be seen in Table 5 along with the χ^2- and p-values. Here, the χ^2 and p-values tell us how well the simulation fits the analytical, expected model. For calculating the χ^2-value, we have assumed that our data points are independent. Unfortunately, our data points are strongly correlated in reality, since the previous snapshot of the universe determines the evolution of the next snapshot. This means that the χ^2-test technically cannot be

used in our case, however the χ^2-value can still be a good indicator of whether the dependency fits our analytical model well. In the case of correlated data, the χ^2-value is expected to be, $\chi^2 < 1$.

	κ	χ^2	p
Uni A, Sim 3	$-6.80 \cdot 10^5$	0.77	0.94
Uni B, Sim 2	$-1.84 \cdot 10^6$	0.12	1
Uni C, Sim 4	$-1.57 \cdot 10^6$	0.47	0.98

Table 5: *The κ-values for Universe A, B and C along with the corresponding χ^2- and p-values.*

From the table, we see that all three universes in general have good p-values, which indicate that our model is a good fit to the acceleration of the Universe, as we also stated above. We see that the p-value for Universe B is actually 1. This is normally a warning that the errorbars are overestimated and since we see that every mean value fits the analytical model with their errorbars, this could be a reason for the exceptionally high p-value.

4.3.1 Calculating the errorbars

The errorbars seen in Figure 33 have been estimated by calculating the standard deviation of the acceleration generated by dark matter for all five simulations of each universe. Since it is easier to assess the deviation of a distribution located around zero, we subtract the normalised analytical acceleration from the data points, since this follows the overall distribution well. This can be seen in Figure 35a for Universe A, where the different colors show the five simulations, with five individual κ-values and the black curve is the analytical acceleration calculated from the Benchmark model. We divide the normalised acceleration generated by dark matter into five equally large bins, which are illustrated by the dashed black lines in Figure 35b. Here, the analytical acceleration has been subtracted from the data points, such that the distribution is located around zero.

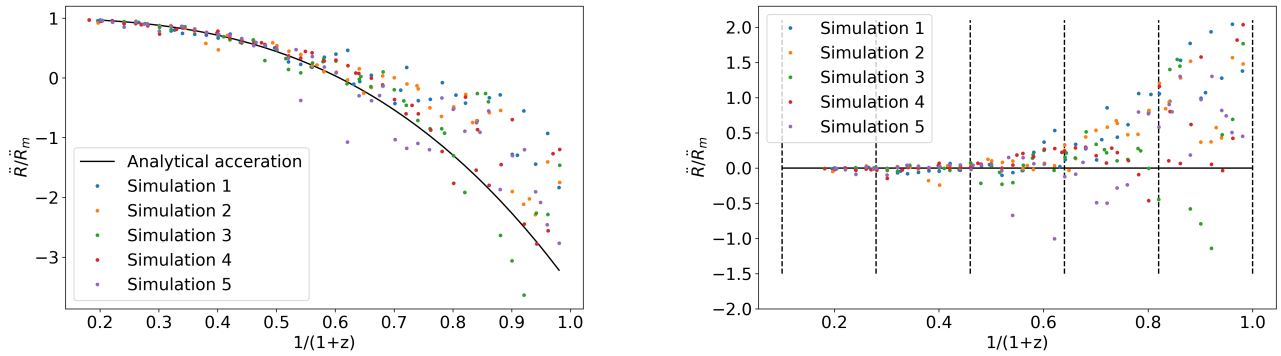

(a) *The distribution of the acceleration generated by dark matter for Universe A.*

(b) *The binning of the acceleration generated by dark matter for Universe A.*

Figure 35: *The distribution of the acceleration generated by dark matter for Universe A along with the binning.*

From Figure 35b it is possible to see that the different simulations lie close to 0 from $1/(1+z) = 0.1$ to $1/(1+z) = 0.45$, but beyond this the simulations start to deviate from the expected line. We calculate the mean and the standard deviation within each bin, and this value is then the uncertainty on the mean value within that bin. The errorbars for all five simulations for Universe A can be seen in Figure 36, where the bold black points represent the mean values of the data points in the bins. Since the scatter increases as the value of $1/(1+z)$ grows in Figure 35b, the standard deviation in the last two bins are larger than the first two. The uncertainties of the first two mean values in Figure 36 are therefore substantially smaller than the last two. The significant deviation that we see between the different simulations result in our large errorbars and our equivalently high p-values.

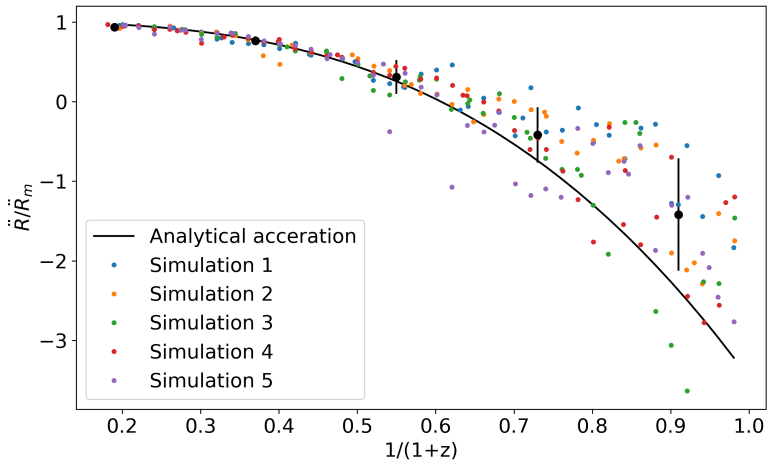

Figure 36: *The normalised acceleration generated by dark matter for all five simulations for Universe A and the bold mean values within each bin with errorbars.*

The errorbars for Universe B and C are found using the same procedure as just described.

4.4 Other possible models

Above we have shown, that we might be able to explain the acceleration of the Universe through our new model, which calculates the acceleration from Equation (3.2.4),

$$\ddot{R}_{DM} = \sum_i -\frac{GM_i}{R_i^2}\left(1 - \kappa\left(\frac{\sigma_i}{c}\right)^2\right),$$

where the acceleration depends on the squared velocity dispersion, σ^2. However, it might be possible to imagine other ways for the acceleration to depend on the velocity dispersion. Below we explore two new varying expressions for the acceleration generated by dark matter and see whether these might be better at explaining the acceleration of the Universe, than our original model.

4.4.1 A simple modification of our model

A simple adjustment of our model could be to vary the power of which the acceleration depends on the velocity dispersion. This new exponent could be any number and because of this, we choose to denote it by x. We can therefore rewrite

Equation (3.2.4), where the velocity dispersion is now raised to the power of x,

$$\ddot{R}_{DM} = \sum_i -\frac{GM_i}{R_i^2}\left(1 - \kappa\left(\frac{\sigma_i}{c}\right)^x\right). \tag{4.4.1}$$

The rest of the equation remains the same as before.

Since we saw that σ^2 was a reasonable fit to the Benchmark model, we look at values of x that are close to two. In Figure 37 we have plotted the acceleration generated by dark matter based on Equation (4.4.1) with $x = 1, 2, 3$.

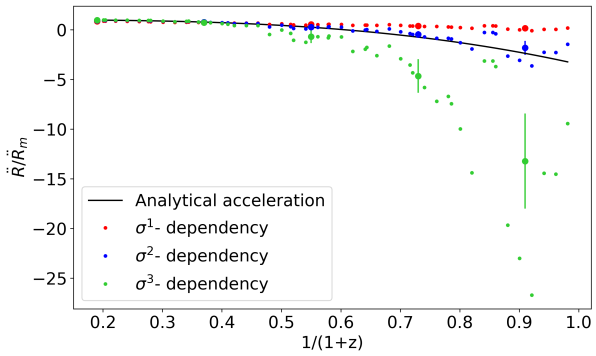

(a) *Universe A, Simulation 3.*

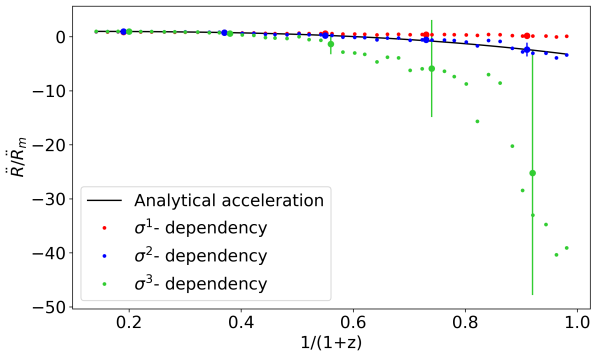

(b) *Universe B, Simulation 2.*

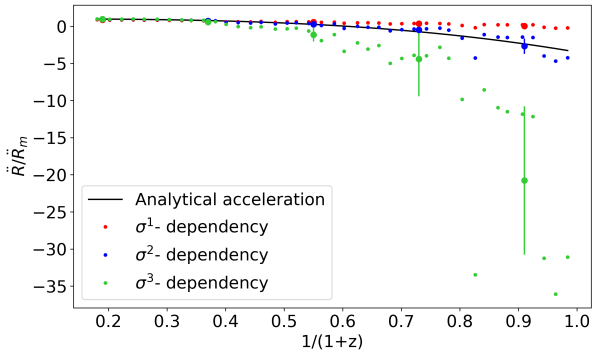

(c) *Universe C, Simulation 4.*

Figure 37: *Our new model with $x = 1, 2, 3$ for our three universes and the normalised analytical acceleration for the Benchmark model.*

The figures 37a, 37b and 37c show the σ^1- (red), σ^2- (blue) and σ^3-dependency (green) for Universe A, B and C, respectively. The bold data points and their

errorbars once again represent the mean value of each of five bins that the data points have been divided into. The κ-values have been calculated in the same way as above in Section 4.3, through Equation (2.2.10), and can be seen in Table 6 along with the χ^2- and p-values of these five mean values.

Common to all three σ^1-dependencies is that they have a p-value of zero. This is due to the fact that they all lie above the normalised analytical acceleration and have small errorbars, making these a poor fit to the Benchmark model. The σ^3-dependencies lie below the analytical model, but since these have very large errorbars compared to the other dependencies, the p-values are above zero, unlike what we saw for the σ^1-dependencies. For Universe B the p-value is 0.69, even though we clearly see a much steeper evolution compared to the analytical comparison model. This could be because of the significantly large errorbars, making it seem like a decent fit. These large errorbars could be due to the fact that the data points are heavily correlated, which also influences the χ^2- and p-values as mentioned in Section 4.3.

		$x = 1$	$x = 3$
Uni A, Sim 3	κ	$-5.04 \cdot 10^2$	$-1.08 \cdot 10^9$
	χ^2	727.92	14.17
	p	0	0.01
Uni B, Sim 2	κ	$-7.79 \cdot 10^2$	$-5.65 \cdot 10^9$
	χ^2	548.26	2.27
	p	0	0.69
Uni C, Sim 4	κ	$-7.67 \cdot 10^2$	$-3.93 \cdot 10^9$
	χ^2	369.89	7.46
	p	0	0.11

Table 6: *The κ-values for Universe A, B and C along with the corresponding χ^2- and p-values for $x = 1$ and $x = 3$.*

As mentioned, the κ-values are found by making sure that our numerical model fits the Benchmark model for $z > 0.6$, where $z = 0.6$ is the redshift at which $\Omega_m = \Omega_\Lambda$. This means that for redshifts higher than $z = 0.6$ our models with $x = 1, 2, 3$ should be tolerable fits to the Benchmark model and it is only for low redshifts, that we are able to see which models should be able to describe the acceleration of the Universe. However, as can be seen in Figure 38, the data points already start to deviate from the Benchmark model at $1/(1 + z) \simeq 0.4$, corresponding to a redshift of $z = 1.5$. This indicates that we should have chosen to fit our models to a smaller range of the Benchmark model, by selecting a limit,

where the influence of Λ was still negligible, which is at redshifts higher than the current value of $z = 0.6$.

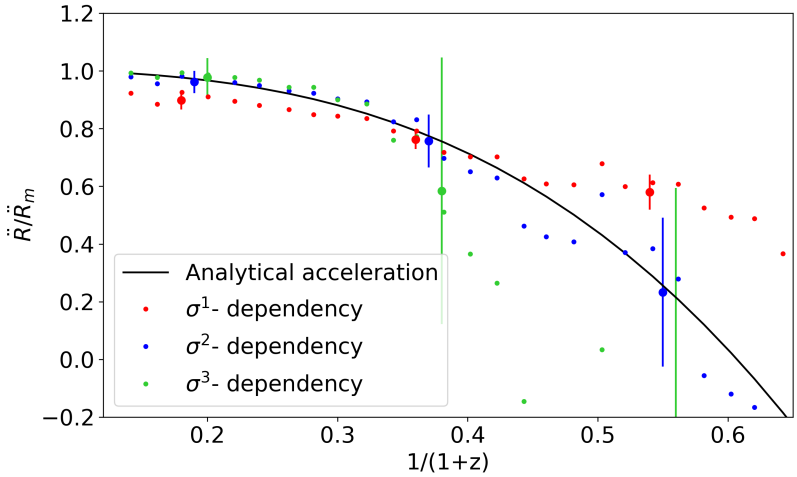

Figure 38: *Our new model with $x = 1, 2, 3$ for our three universes and the normalised analytical acceleration for the Benchmark model for high redshifts.*

The errorbars for the acceleration generated by dark matter depending on the velocity dispersion to a power of $x = 1$ and $x = 3$ have been calculated in the same way as for $x = 2$, which is explained in Section 4.3.1. This is done by finding the standard deviation for all five simulations of each universe in five equally large bins. For $x = 2$ we subtracted the Benchmark model from our data points in order to get a distribution located around zero. However, to obtain a similar distribution for $x = 1$, we have instead subtracted a straight line that fits the distribution of the data points across all five bins. This can be seen in Figure 39a. For $x = 3$ we find five straight lines that fit the distributions within each bin and subtract these from the respective data points, which can be seen in Figure 39b.

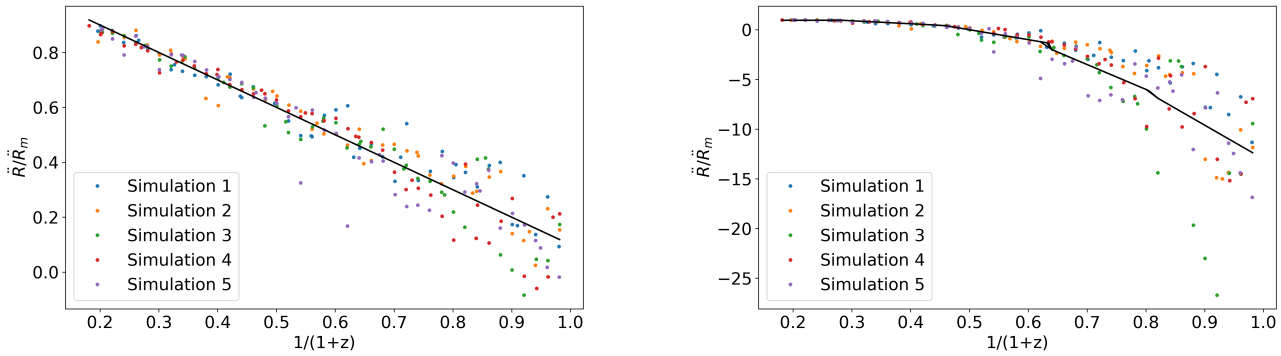

(a) $x = 1$ (b) $x = 3$

Figure 39: *The distribution of the acceleration generated by dark matter with* $x = 1$ *and* $x = 3$ *for Universe A.*

The reason for extending our original model to include other exponents of the velocity dispersion, was to explore whether there might be some values of x that could make the acceleration generated by dark matter a better fit to the Benchmark model. However, in Figure 37 we saw that the acceleration with $x = 2$ was still the best fit. We therefore wish to examine values of x closer to two, by varying it slightly such that we now try $x = 7/4$ and $x = 9/4$.

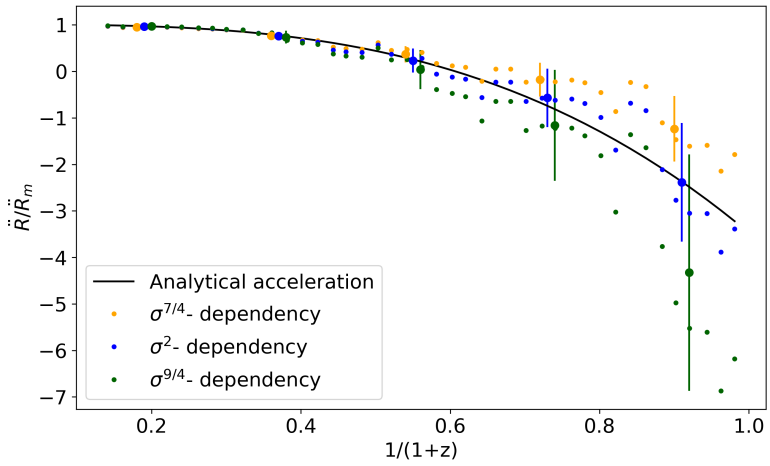

Figure 40: *Our new model with* $x = 7/4$, $x = 2$ *and* $x = 9/4$ *for our three universes and the normalised analytical acceleration for the Benchmark model. The mean values of the model with* $x = 7/4$ *and* $x = 9/4$ *have been shifted slightly to the left and right, respectively.*

Figure 40 shows the acceleration generated by dark matter with $x = 7/4$ (orange), $x = 2$ (blue) and $x = 9/4$ (dark green) for Universe B, Simulation 2. The mean values of the $\sigma^{7/4}$- and $\sigma^{9/4}$-dependency have been shifted slightly to the left and right, respectively, in order to distinguish the errorbars from each other. The κ-values and the belonging χ^2- and p-values of the data points can be seen in Table 7. The errorbars for the $x = 7/4$ and $x = 9/4$ models have been found in the same way as the errorbars for the $x = 3$ model with five straight lines.

We see, that the $\sigma^{7/4}$-dependency lies above the analytical model and has small errorbars, which leads to a p-value of 0.31. On the other hand, the $\sigma^{9/4}$-dependency lies below the expected curve, but because of the large errorbars, it still has a p-value of 0.88. Had we not shifted the mean values, we would see that the different models would overlap, which means that we cannot distinguish these from each other, making us unable to determine the value of x more accurately. This means, that an acceleration generated by dark matter with $x = 2$ is our best prediction for a model to explain the acceleration of the Universe, at this point in time.

	$x = 7/4$	$x = 2$	$x = 9/4$
κ	$-2.59 \cdot 10^5$	$-1.84 \cdot 10^6$	$-1.32 \cdot 10^7$
χ^2	4.82	0.12	1.18
p	0.31	1	0.88

Table 7: *The κ-values for Universe B, Simulation 2 with $x = 7/4$, $x = 2$ and $x = 9/4$ along with the corresponding χ^2- and p-values.*

4.4.2 Extending our model further

By additionally expanding our model, we can imagine that the acceleration generated by dark matter does not only depend on the velocity dispersion of the halos within the sphere, but also the halo on the edge of the sphere. This scenario can be seen in Figure 41, where the velocity dispersion of the halo on the edge of the sphere (cyan) is also taken into account.

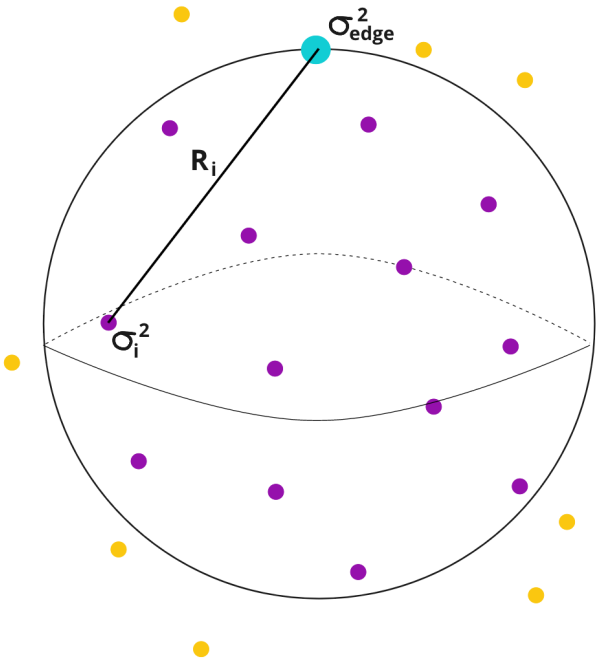

Figure 41: *An illustration of a halo on the edge of the sphere (cyan) with velocity dispersion, σ_{edge}, and the halos within the sphere (purple) with velocity dispersion, σ_i, and distance to the halo on the edge, R_i. Halos outside the sphere are colored orange.*

By considering two different velocity dispersion, we can now have two different exponents, such that the velocity dispersion of the halos within the sphere, σ_i, is raised to the power of x and the velocity dispersion of the halo on the edge of the sphere, σ_{edge} is raised to the power of y. This allows us to explore even more complicated versions of our model to see if this is a better fit to the acceleration of the Universe. The simple model only depending on σ_i is given by Equation (4.4.1),

$$\ddot{R}_{DM} = \sum_i -\frac{GM_i}{R_i^2}\left(1 - \kappa\left(\frac{\sigma_i}{c}\right)^x\right).$$

If we include both the velocity dispersions of the halos inside of the sphere, σ_i and the halo on the edge of the sphere, σ_{edge}, the extended model becomes,

$$\ddot{R}_{DM} = \sum_i -\frac{GM_i}{R_i^2}\left(1 - \kappa\left(\frac{\sigma_i^x \sigma_{edge}^y}{c^{(x+y)}}\right)\right), \tag{4.4.2}$$

where x is the power of σ_i and y is the power of σ_{edge}. In order to make this term dimensionless, we divide by $c^{(x+y)}$.

If we look at different values of x and y, we see that when $x, y = 0$, the model describing the acceleration generated by dark matter reduces to the classic gravitational acceleration from Equation (3.2.1),

$$\ddot{R}_m = \sum_i -\frac{GM_i}{R_i^2}.$$

Keeping $y = 0$ but letting $x > 0$, it describes the simple model explained through Equation (4.4.1), since σ_{edge} becomes one. If we instead put $x, y = 1$, we get a case similar to the Lorentz force, since this depends on two different velocities.

Setting $x, y > 0$ we can test the extended model both by letting $x = y$ and $x \neq y$ and see if any of these can create a better fit to the Benchmark model. In Figure 42 the extended model for the acceleration generated by dark matter with $x, y = 1$ (red), $x, y = 3/2$ (blue) and $x, y = 2$ (green) can be seen along with the Benchmark model (black). The κ-values and their belonging χ^2- and p-values can be seen in Table 8.

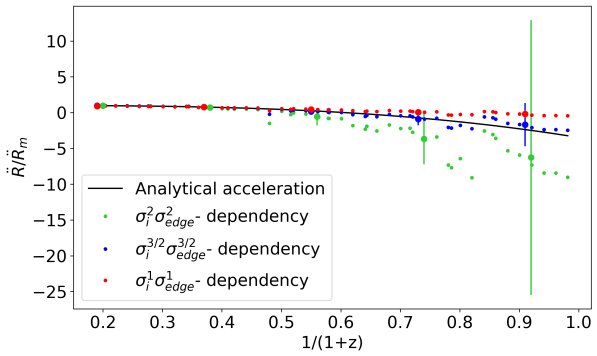

(a) *Universe A, Simulation 3.*

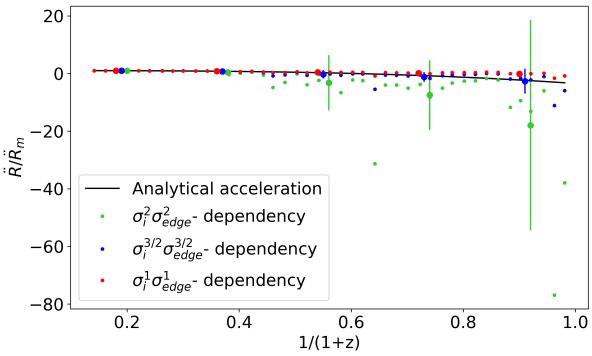

(b) *Universe B, Simulation 2.*

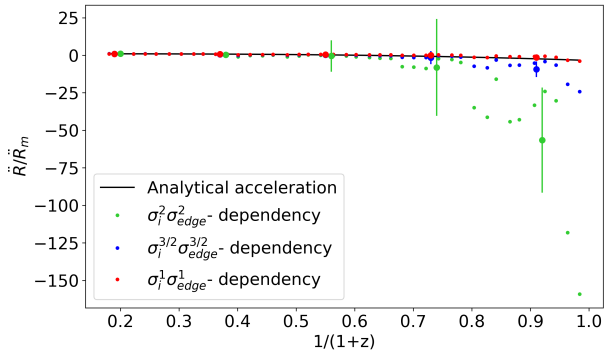

(c) *Universe C, Simulation 4.*

Figure 42: *Our extended model with $x, y = 1$, $x, y = 2$ and $x, y = 3/2$ for our three universes and the normalised analytical acceleration for the Benchmark model.*

For Universe A and B the $x, y = 1$ model is a poor fit, since the data points all lie above the expected line and the mean values have small errorbars. This unsuitable fit can also be seen from the low p-values. The dependency for Universe C, has a much better p-value, on the other hand, since it lies closer to the anticipated model than the other two universes.

		$x, y = 1$	$x, y = 3/2$	$x, y = 2$
Uni A,	κ	$-1.40 \cdot 10^{6}$	$-7.05 \cdot 10^{12}$	$-2.17 \cdot 10^{9}$
Sim 3	χ^2	24.50	0.22	2.42
	p	$6.33 \cdot 10^{-5}$	0.99	0.66
Uni B,	κ	$-4.15 \cdot 10^{6}$	$-1.70 \cdot 10^{10}$	$-9.06 \cdot 10^{13}$
Sim 2	χ^2	16.30	0.39	1.01
	p	$2.65 \cdot 10^{-3}$	0.98	0.91
Uni C,	κ	$-2.96 \cdot 10^{6}$	$-9.00 \cdot 10^{13}$	$-3.15 \cdot 10^{6}$
Sim 4	χ^2	3.11	2.30	3.09
	p	0.54	0.68	0.54

Table 8: *The κ-values for Universe A, B and C along with the corresponding χ^2- and p-values for $x, y = 1$, $x, y = 3/2$ and $x, y = 2$.*

Looking at the p-values for the model with $x, y = 2$, we see that they all lie above 0.50, indicating that this model should be a good candidate for the fit. However, these high values are caused by the large errorbars on the mean values and by eye, it is possible to determine that the $x, y = 2$ model in general is a poor fit to the Benchmark model. The p-values for the model with $x, y = 3/2$ also lie above 0.5, but opposite to the model with $x, y = 2$, it is difficult to determine whether the $x, y = 3/2$ model is a good fit by just looking at the figure and we instead show it by itself in Figure 43.

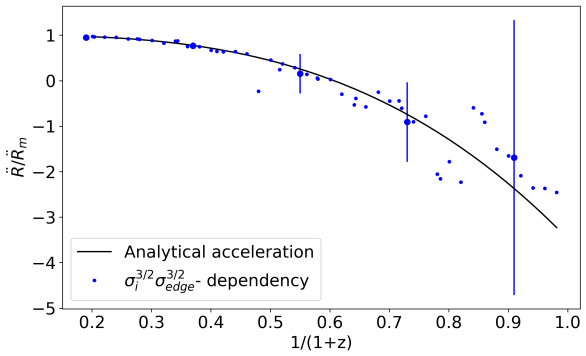

(a) *Universe A, Simulation 3.*

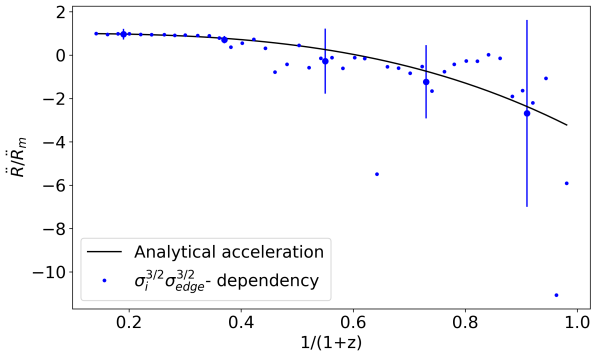

(b) *Universe B, Simulation 2.*

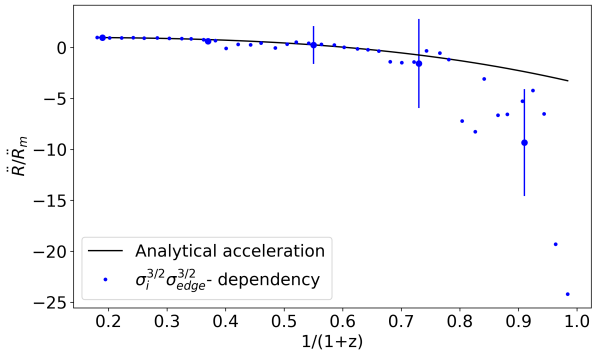

(c) *Universe C, Simulation 4.*

Figure 43: *Our extended model with $x, y = 3/2$ for our three universes and the normalised analytical acceleration for the Benchmark model.*

By looking at Figure 43 we see that the model for the acceleration generated by dark matter with $x, y = 3/2$ seems to be a reasonable fit when looking at Universe A and B, but the tail end of the graph showing the model for Universe C diverges from the Benchmark model. This can also be seen from the p-value, which is much less than the p-value of the models for the other two universes.

We now try looking at the case where $x \neq y$ and Figure 44 shows the extended model for the acceleration generated by dark matter with $x = 2, y = 1$ (purple) and $x = 1, y = 2$ (orange) along with the Benchmark model (black). The κ-values and their belonging χ^2- and p-values can be seen in Table 9.

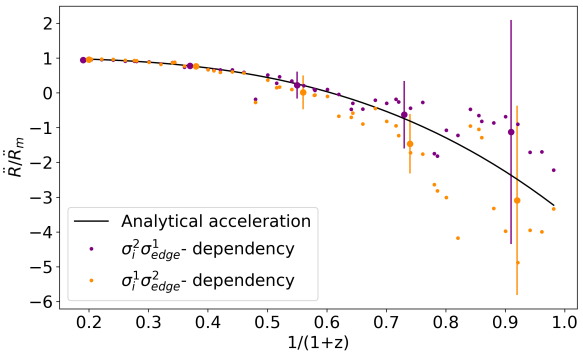

(a) *Universe A, Simulation 3.*

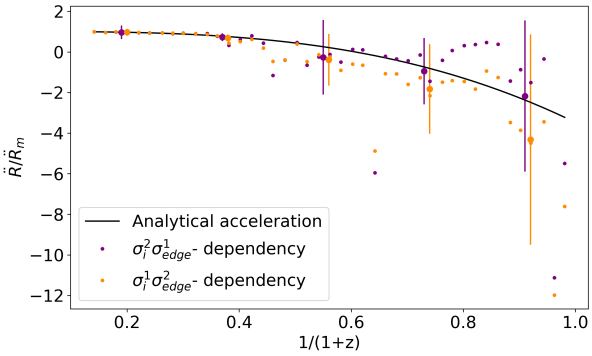

(b) *Universe B, Simulation 2.*

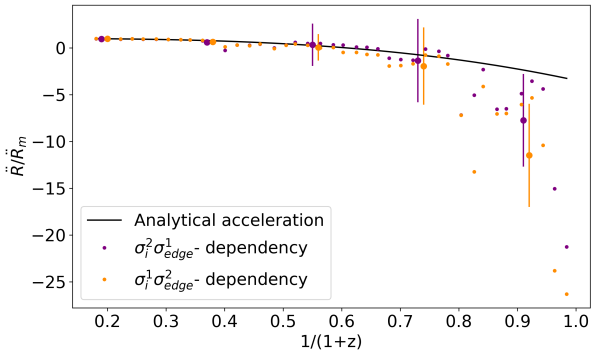

(c) *Universe C, Simulation 4.*

Figure 44: *Our extended model with $x = 2, y = 1$ and $x = 1, y = 2$ for our three universes and the normalised analytical acceleration for the Benchmark model.*

From looking at Figure 44, it would seem as if the data points follow the tendency of the Benchmark model, but there is no clear pattern between the three universes, and it is therefore difficult to conclude anything that applies to all simulations. This could be due to the fact that this extended model is more complicated than the simple model, that only contains one velocity dispersion, and we would therefore need better statistics in order to determine how well the data fits the expected model.

		$x = 1, y = 2$	$x = 2, y = 1$
Uni A, Sim 3	κ	$-3.87 \cdot 10^9$	$-2.98 \cdot 10^9$
	χ^2	1.58	0.15
	p	0.81	0.99
Uni B, Sim 2	κ	$-1.27 \cdot 10^{10}$	$-2.12 \cdot 10^{10}$
	χ^2	0.93	0.17
	p	0.92	1
Uni C, Sim 4	κ	$-7.05 \cdot 10^9$	$-1.08 \cdot 10^{10}$
	χ^2	3.34	1.79
	p	0.50	0.77

Table 9: *The κ-values for Universe A, B and C along with the corresponding χ^2- and p-values for $x = 1, y = 2$ and $x = 2, y = 1$.*

The errorbars, used in the figures in this section, have been calculated in the same way as the errorbars for Section 4.3.1 involving only one velocity dispersion dependency. Here, the errorbars for the $x, y = 1$ model was found from fitting a single straight line across the five bins, while the errorbars for the other four models was found by fitting five straight lines to each of the five bins.

The simulations, that have not been shown throughout this Results-section, can be seen in the Appendix.

5 Discussion

In this section, we wish to discuss the results of our work and the limitations involved in the finding of these. Potential ways of improving the results, and actions that could be taken in the future are also looked into, along with a possible explanation for our proposed model.

5.1 Our results

The acceleration of the Universe has been observed through measurements of supernovae and baryonic acoustic oscillations, as described in Section 1.1. The Benchmark model is a generally accepted theory that allows us to describe the physics and observations of our Universe. By looking at all of our simulations, we see that the acceleration generated by dark matter follows the tendency of the analytical acceleration of the Benchmark model, which means that our new model might be a possible candidate to explain the acceleration of the Universe, without the cosmological constant, Λ. As a reminder, our new general model is given by Equation (4.4.2),

$$\ddot{R}_{DM} = \sum_i -\frac{GM_i}{R_i^2}\left(1 - \kappa\left(\frac{\sigma_i^x \sigma_{edge}^y}{c^{(x+y)}}\right)\right).$$

From analysing our results, we see that in general, it is easier to asses the graphs showing the acceleration generated by dark matter only depending on a single velocity dispersion, where $y = 0$. For the models with $x = 1, 2, 3$, it is clear to see which are close to the Benchmark model and which vary to a greater or lesser extent. The p-values of the model with $x = 1$ are all zero, as stated in Table 6 in Section 4.4.1, and based on the clearly poor fits and small errorbars, as can be seen in Figure 37 in Section 4.4.1, we are able to dismiss this as a possible explanation for the acceleration of the Universe. We also saw that the model with $x = 3$ was a poor fit, but unfortunately due to misleading statistics and p-values above zero, as shown in Table 6, we are not able to outright reject this model. However, by eye it is possible to see, that this model is not a good candidate as a fit to the acceleration of the Universe.

The most promising model seems to be our original model with $x = 2$, since these data points follow the tendency of the Benchmark model and the p-values are close to one, which is shown in Table 5 in Section 4.3. When looking at values of x close to $x = 2$, like $x = 7/4$ and $x = 9/4$, we are unable to distinguish between any of these models as the best fit, since these overlap, as can be seen in Figure 40 in Section 4.4.1. Had we produced several, additional simulations of our three

universes, we would have been able to minimize the size of the errorbars, which would make it easier to tell the difference between the three models. By doing this we could possibly find a more accurate value of x that enables our model to potentially explain the acceleration of the Universe.

In contrast, the plots showcasing the model for the acceleration containing two different velocity dispersions, where $y \neq 0$, are much more difficult to determine anything useful from. Based on the p-values from Table 8 and 9 in Section 4.4.2 and the appearance of the models in Figure 42 and 44 in Section 4.4.2, we are unable to reject any of the models. A way of possibly getting around this, could be to create even more simulations of the universes we have already generated, along with making additional universes with other parameters. This would improve the statistics of our simulations and might make it possible for us to see a general tendency.

5.2 Limitations of our simulations

Working with a simulated model of our Universe, we are limited by the capability of computers. The Universe is infinitely large with an extreme amount of particles, which is beyond the scope of any computer. However, as stated in Section 2.3, a small, contained version of the Universe can be a useful replica for determining the physics of the Universe. We are still interested in creating a simulation as close to the actual Universe as possible, which means that large amounts of particles and overall bigger simulations are preferred. It would have been possible to create much bigger simulations than what we have produced, since we have access to a cluster of computers that is able to generate the simulations in a reasonable amount of time. However, when we wish to analyse these simulations, we are limited by the program used for executing our code, meaning that the analysis of a large simulation would take an unreasonable amount of time. We therefore chose to quantify our results by making several smaller simulations instead of qualifying a single big simulation.

As stated above, bigger simulations are generally preferred when looking at the large scale structure of the Universe. However, when choosing a large amount of particles and a big volume, it compromises the resolution on smaller scales, such as when looking at the inner workings of a galaxy. A better resolution on these scales can be obtained by creating smaller simulations, where the particle amount is kept the same but the volume is much smaller. It is therefore necessary to consider the kind of simulation needed for the given analysis and the results one wishes to produce. In our case, knowledge about the galaxies on their own is not interesting, and we are instead looking for information about the dark matter

halos and the large scale structure. This makes a big simulation preferable to us, as already mentioned. If one wishes to explore both the small and large scales of the Universe at the same time, it could be necessary to combine two or several simulations with different conditions.

In our simulations we have kept the Λ-component intact, by letting $\Omega_\Lambda = 0.69$, even though this component should be absent according to our new model. This is done since we still need the effect of dark energy to influence the evolution of the simulations. In an ideal scenario, we would have to calculate Ω_Λ for each redshift and let this determine the evolution of the next snapshot. In this case, we would let $\Omega_\Lambda = 0.69$ for the initial snapshot. Once this has been produced, we can calculate the acceleration generated by dark matter, $\ddot{R}_{DM}$, and from this determine the new value of Ω_Λ needed for producing the next snapshot. Even though calculating Ω_Λ for each redshift is fairly straightforward, implementing this in the code, used for creating the next timestep, is not trivial. Due to the complexity of changing this component, we have not explored this further. This could be an interesting task to look into in the future.

5.3 Observations in the future

The only way of definitively confirming whether our model could be a possible explanation for the acceleration of the Universe, is by comparing our new model with actual observations of the Universe, instead of just the theoretical Benchmark model. We have described how dark energy and the acceleration of the Universe has been observed through observations of CMB, supernovae and baryonic acoustic oscillations. We want our model to be able to describe the Universe as it has already been observed, which we have tried to do by making sure that our model is in agreement with the Benchmark model. However, in the future we expect that there should be a clear distinction between the Benchmark model and our model, as it was shown in Figure 13, which can be seen again below.

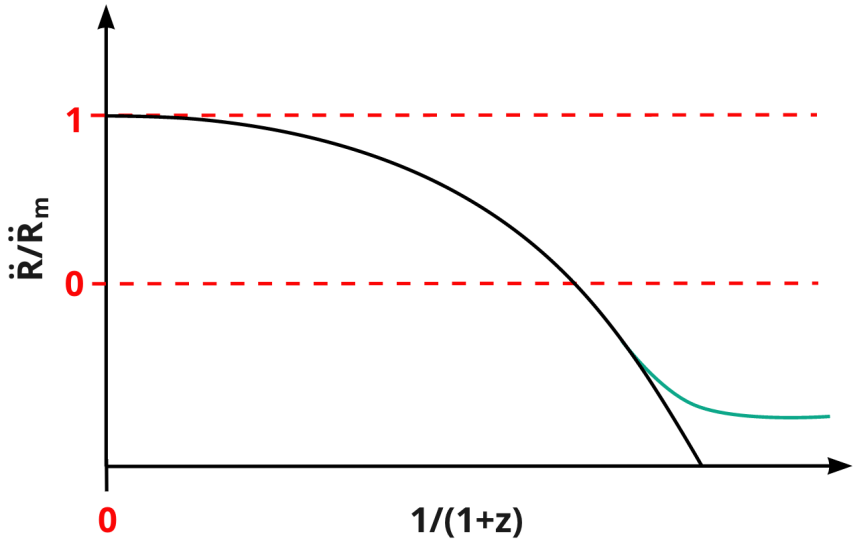

In the figure, the normalised acceleration of the Universe according to the Benchmark model can be seen as the black line. The green line indicates where our model will deviate from the analytical Benchmark model. At the moment, we are not able to see a difference between the two models, which is why we have created our model such that it fits the Benchmark model. But as time passes, it should be possible to tell the two apart, since our model depends on structure formation, which evidently will stop, as we saw through the equations of Section 2.2.1. When structure formation ends, the velocity dispersion of the dark matter halos, σ, stop increasing, which in turn makes our new force and thereby acceleration constant.

In order to be able to properly measure this distinction in the future, we need actual observations to confirm our model. One way of observing this difference, is through observations of type Ia supernovae. In Section 1.1 we described how observation of supernovae have helped confirm that we live in an accelerating universe, through Figure 3. Below, a rough sketch, based on this figure, can be seen in Figure 45.

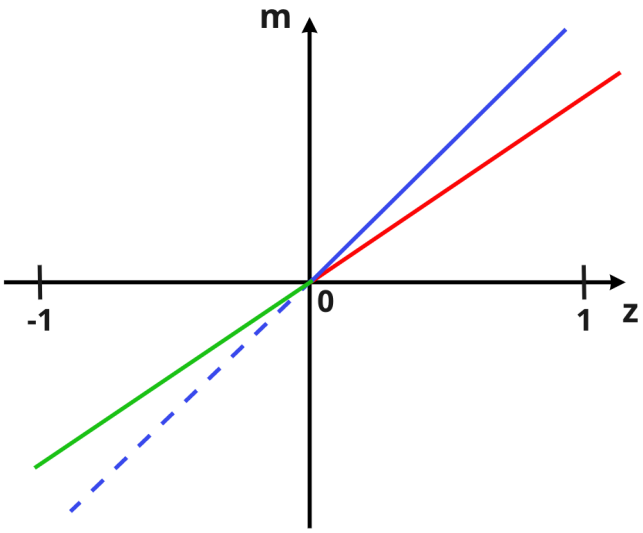

Figure 45: *A sketch of the apparent magnitude, m, of type Ia supernovae as a function of redshift, z. The blue solid line is a model of a universe with dark energy, whereas the red line describes a universe without. The blue dashed line illustrates the continuation of the model with dark energy in the future and the green line shows what we expect the observations to look like in the future, if our model is true.*

This figure shows a model of how observed magnitudes of supernovae depend on their redshift, where the solid blue line describes a model with dark energy, while the red line shows a model without. Both of these models end at today's redshift of $z = 0$. In a universe where the cosmological constant describes dark energy, the relationship between observed magnitudes and redshift should continue on as the dashed blue line. However, if our model is correct, the relationship will change, since the difference between the observed magnitudes becomes less for each redshift, as the acceleration of the Universe slows down. At this point, we do not know at what redshift we should be able to see a distinction between the two models. This could just as well be at $z = -1$, as it could be at $z = -10$. Only time will tell.

Since the simulations we are working with show the evolution of the Universe from $z = 20$ to $z = 0$, we have not been able to see this clear difference between our new model and the Benchmark model. It would therefore be ideal to create a simulation that could show the future of the Universe, to see whether the simulated data will follow our new model or the Benchmark model. However, since the observable distinction between the two models in the future remains a speculation, we have

chosen not to look further into creating these simulations and have instead chosen to find the best model for describing the current Universe. This could be an interesting path to go down in future work.

5.4 Possible explanation

At large scales we see structures such as galaxies and galaxy clusters moving away from each other due to the acceleration of the Universe being larger than the gravitational acceleration. Therefore we need the newly proposed force created by the movement of dark matter particles in dark matter halos to be larger than the gravitational acceleration as well. For this to work, the dark matter particles in a galaxy should move around and create this new force, which should repel other galaxies, leaving us with a larger repulsive force than the attractive force. However, the effects of this force should only be seen on large scales. When looking at small scales, such as the components of a galaxy or a solar system, we see that these are held together by gravity and are not affected by this repulsion. If the force was greater than the gravitational acceleration on small scales too, structures such as dwarf galaxies would not be able to exist, since these are dark matter dominated, such that the repulsive force would make it impossible for them to gather. The new force must for that reason only work on large scales, where we see galaxies with great distances between them being pulled from each other as well as galaxy clusters being separated further.

In order to make this happen, we can introduce a screening-term, like the one known from electromagnetism. Contrary to the effect we want to see, the screening term in electromagnetism causes an effect on small scales that disappears as the distance grows, which can be seen in Figure 46a. We are instead interested in seeing an effect on large scales that fades when looking at small distances, as is shown in Figure 46b.

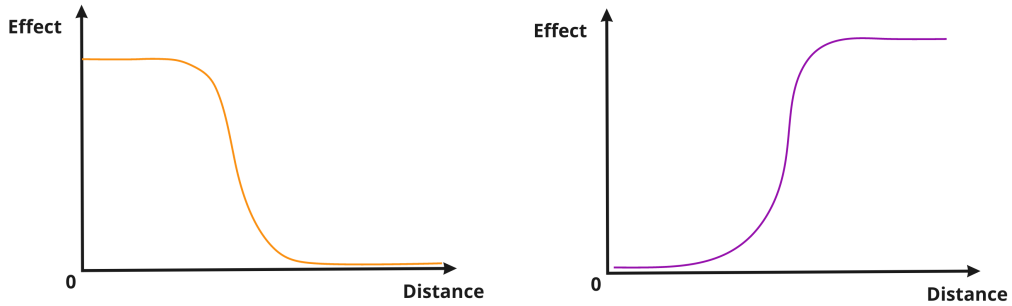

(a) *Electromagnetic case.* (b) *Our case.*

Figure 46: *A sketch of how the effect depends on the distance.*

To account for this effect and make sure that the new force only applies on large scales, we can introduce two new exchange forces and their related particles. We already know that dark matter creates a gravitational field, due to the observed gravitational acceleration. Aside from this, we might also be able to imagine that dark matter could produce two other fields, similar to that of the gravitational one. These two fields can be seen in Figure 47, depicted by the blue and red arrows surrounding the halo in the center (black dot).

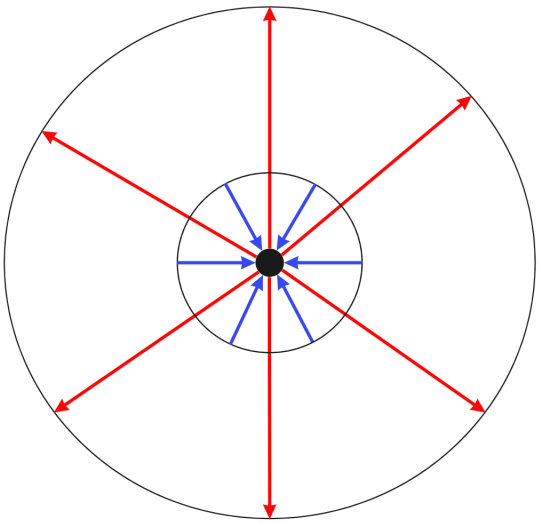

Figure 47: *A sketch of two opposite force-fields surrounding a dark matter halo (black dot), where the blue field cancels out the red field on small scales.*

These two fields in the figure should work, such that on small scales the two fields work exactly opposite each other and thereby cancel each other out. On large scales on the other hand, we need for one of the fields to disappear. If the blue field fades, it leaves only the red field behind, which creates the outward force, that might be the cause of the acceleration that we can observe today. In order for this to happen, the blue field must produce a force-carrying particle with a mass. Since the particle has a mass, it hinders the particle from working on infinite distances, resulting in the disappearance of the blue field. In the normal case of exchange forces in electromagnetism, the particles that are produced are massless, resulting in a force that theoretically should work on infinite distances. Since this describes the kind of force we are interested in finding, we imagine that the non-fading field, the red field, should be of this kind. The scale at which the blue field should disappear is unsure, but we know that it should be greater than the radius of a galaxy cluster of a few Mpc[55], since these are kept together by gravity.

[55]Sparke, L. S. and Gallagher III, J. S. 2007.

6 Conclusion

With our thesis, we have found that it could be possible to describe the acceleration of the Universe through forces generated by dark matter, excluding the theoretical cosmological constant, Λ. Our model is based on the movement of dark matter particles in dark matter halos, where a velocity dispersion arises due to the individual motions of the particles. This force should work such that on small scales, gravity dominates and allows for the structures to be kept together, whereas on large scales, the new, repulsive force should drag the Universe apart, giving us an accelerating universe.

The acceleration, $\ddot{R}_{DM}$, has been thought out as an extension of the classic gravitational acceleration, such that for a dark matter halo, located on the edge of a sphere containing a number of halos, the acceleration is of the form,

$$\ddot{R}_{DM} = \sum_i -\frac{GM_i}{R_i^2}\left(1 - \kappa\left(\frac{\sigma_i^x \sigma_{edge}^y}{c^{(x+y)}}\right)\right),$$

where M_i is the mass of the halos within the sphere, R_i is the distance from the halo on the edge of the sphere to a given halo within, κ is a dimensionless scaling factor, c is the speed of light, σ_i is the velocity dispersion of the halos within the sphere and σ_{edge} is the velocity dispersion of the halo on the edge of the sphere. x and y are exponents of the velocity dispersions and can be of any value.

We have tested models with different values of x and y, allowing us to examine models with varying velocity dispersion dependencies, to see if they can explain the acceleration of the Universe. Since the generally accepted theory that explains this acceleration is the Benchmark model, we use this model as a comparison for our own proposed model. We have used the acceleration equation, derived from the Friedmann equation, with cosmological parameters according to the Benchmark model, $\Omega_{r,0} = 9 \cdot 10^{-5}$, $\Omega_{m,0} = 0.31$ and $\Omega_{\Lambda,0} = 0.69$[56,57]. In order for us to test our model we have created several numerical simulations of a universe with the parameters just stated.

With the numerical simulations we have examined different models of the acceleration generated by dark matter, in order to see if any of these can explain the acceleration of the Universe. It was difficult to draw a conclusion from the models with $x, y \neq 0$, since the different models did not follow an overall tendency. With better statistics, it could be possible to see a general trend and conclude which

[56] Collaboration 2018.
[57] Ryden 2017.

models can explain the acceleration of the Universe. Because of the poor fit to the Benchmark model and the p-values of zero, the model with $x = 1, y = 0$ can be easily rejected. Similarly, the model with $x = 3, y = 0$ was also a bad fit to the Benchmark model, but since the p-values are above zero, due to the large errorbars, this model cannot be rejected. We found that the best model to describe the acceleration of the Universe, according to the Benchmark model, is the model with $x = 2, y = 0$. However, we discovered that we were not able to distinguish values of x close to $x = 2$, and therefore it is possible that the true value of x differs slightly from this value.

References

Allen, S. W. et al. (June 2003). "Cosmological constraints from the local X-ray luminosity function of the most X-ray-luminous galaxy clusters". In: *Monthly Notices of the Royal Astronomical Society* 342.1, pp. 287–298. ISSN: 1365-2966. DOI: 10.1046/j.1365-8711.2003.06550.x. URL: http://dx.doi.org/10.1046/j.1365-8711.2003.06550.x.

Baugh, C. M. (Nov. 2006). "A primer on hierarchical galaxy formation: the semi-analytical approach". In: *Reports on Progress in Physics* 69.12, pp. 3101–3156. ISSN: 1361-6633. DOI: 10.1088/0034-4885/69/12/r02. URL: http://dx.doi.org/10.1088/0034-4885/69/12/R02.

Berger, M. J. and Colella, P. (May 1989). "Local Adaptive Mesh Refinement for Shock Hydrodynamics". In: *Journal of Computational Physics* 82.1, pp. 64–84. DOI: 10.1016/0021-9991(89)90035-1.

Binney, J. and Tremaine, S. (2008). *Galactic Dynamics*. Second. Princeton University Press.

Birrell, J., Yang, C. T., and Rafelski, J. (Jan. 2015). "Relic neutrino freeze-out: Dependence on natural constants". In: *Nuclear Physics B* 890, pp. 481–517. ISSN: 0550-3213. DOI: https://doi.org/10.1016/j.nuclphysb.2014.11.020. URL: http://www.sciencedirect.com/science/article/pii/S0550321314003642.

Coles, P. and Lucchin, F. (2002). *Cosmology, The Origin and Evolution of Cosmic Structure*. Second. John Wiley & Sons, Ltd.

Collaboration, Planck (July 2018). *Planck 2018 results. I. Overview and the cosmological legacy of Planck*. arXiv: 1807.06205 [astro-ph.CO].

de Bernardis, P. et al. (Jan. 2002). "Multiple Peaks in the Angular Power Spectrum of the Cosmic Microwave Background: Significance and Consequences for Cosmology". In: *The Astrophysical Journal* 564.2, 559?566. ISSN: 1538-4357. DOI: 10.1086/324298. URL: http://dx.doi.org/10.1086/324298.

Dehnen, W. and Read, J. I. (May 2011). "N-body simulations of gravitational dynamics". In: *The European Physical Journal Plus* 126.5. ISSN: 2190-5444. DOI: 10.1140/epjp/i2011-11055-3. URL: http://dx.doi.org/10.1140/epjp/i2011-11055-3.

Dinculescu, A. (Jan. 2007). "On the energy density of the cosmic microwave background". In: *Astrophysics and Space Science* 310, pp. 237–239. DOI: 10.1007/s10509-007-9507-7.

Eisenstein, D. J. and Hut, P. (May 1998). "HOP: A New Group-Finding Algorithm for N-Body Simulations". In: *The Astrophysical Journal* 498.1, pp. 137–142. ISSN: 1538-4357. DOI: 10.1086/305535. URL: http://dx.doi.org/10.1086/305535.

ESA - Cosmic Microwave Background (n.d.). https://www.esa.int/ESA_Multimedia/Images/2013/03/Planck_CMB. Accessed: 2020-07-22.

Evolution of the Universe (n.d.). https://jila.colorado.edu/~ajsh/courses/astr3740_19/evol.html. Accessed: 2020-07-24.

Faessler, A. et al. (Jan. 2017). "Can one measure the Cosmic Neutrino Background?" In: *International Journal of Modern Physics E* 26.01n02, p. 1740008. ISSN: 1793-6608. DOI: 10.1142/s0218301317400080. URL: http://dx.doi.org/10.1142/S0218301317400080.

Fisenko, A. and Lemberg, V. (Jan. 2014). "On the radiative and thermodynamic properties of the Cosmic Microwave Background radiation using COBE FIRAS instrument data". In: *Astrophysics and Space Science* 352. DOI: 10.1007/s10509-014-1884-0.

Freedman, R. A. et al. (2014). *Universe*. Tenth. W H Freeman & Co.

Griffiths, D. J. (2013). *Introduction to Electrodynamics*. fourth. Pearson.

Hahn, O. and Abel, T. (July 2011). "Multi-scale initial conditions for cosmological simulations". In: *Monthly Notices of the Royal Astronomical Society* 415.3, pp. 2101–2121. ISSN: 0035-8711. DOI: 10.1111/j.1365-2966.2011.18820.x. URL: http://dx.doi.org/10.1111/j.1365-2966.2011.18820.x.

Halo Finding and Analysis (n.d.). https://yt-project.org/doc/analyzing/analysis_modules/halo_catalogs.html?fbclid=IwAR2_ED6i1i83tUsO8u96f8zo5wlAIz0xHOBahKNo1sm_zK-NV5HNXWylbAk-hop-finding. Accessed: 2019-11-27.

Hubble Ultra Deep Field (n.d.). https://hubblesite.org/image/3886/category/58-hubble-ultra-deep-field. Accessed: 2020-07-28.

Kowalski, M. et al. (Oct. 2008). "Improved Cosmological Constraints from New, Old, and Combined Supernova Data Sets". In: *The Astrophysical Journal* 686.2, pp. 749–778. ISSN: 1538-4357. DOI: 10.1086/589937. URL: http://dx.doi.org/10.1086/589937.

Kragh, H. (Nov. 2011). *Preludes to dark energy: Zero-point energy and vacuum speculations*. arXiv: 1111.4623 [physics.hist-ph].

Kuzkin, V. A. (Sept. 2014). "On angular momentum balance for particle systems with periodic boundary conditions". In: *ZAMM - Journal of Applied Mathematics and Mechanics / Zeitschrift fur Angewandte Mathematik und Mechanik* 95.11, pp. 1290–1295. ISSN: 0044-2267. DOI: 10.1002/zamm.201400045. URL: http://dx.doi.org/10.1002/zamm.201400045.

Martizzi, D. (2019). *Lecture Notes from the course Gravitational Dynamics and Galaxy Formation*. Niels Bohr Institute, University of Copenhagen.

Peacock, J. A. and the 2dFGRS Team (May 2001). "Measuring Large-Scale Structure with the 2dF Galaxy Redshift Survey". In: *ESO ASTROPHYSICS SYM-*

POSIA, pp. 221–230. DOI: 10.1007/10854354_63. URL: http://dx.doi.org/10.1007/10854354_63.

Perlmutter, S. (Apr. 2000). "Supernovae, dark energy and the accelerating universe". In: *Physics Today* 56. DOI: 10.1063/1.1580050.

Planck's Power Spectrum of Temperature Fluctuations in The Cosmic Microwave Background (n.d.). https://sci.esa.int/web/planck/-/51555-planck-power-spectrum-of-temperature-fluctuations-in-the- cosmic-microwave-background. Accessed: 2020-07-27.

Ryden, B. (2017). *Introduction to Cosmology*. Second. Cambridge University Press.

Sparke, L. S. and Gallagher III, J. S. (2007). *Galaxies in the Universe*. Second. Cambridge University Press.

Teyssier, R. (Apr. 2002). "Cosmological hydrodynamics with adaptive mesh refinement". In: *Astronomy & Astrophysics* 385.1, pp. 337–364. ISSN: 1432-0746. DOI: 10.1051/0004-6361:20011817. URL: http://dx.doi.org/10.1051/0004-6361:20011817.

Turk, M. J. et al. (Dec. 2010). "yt: A MULTI-CODE ANALYSIS TOOLKIT FOR ASTROPHYSICAL SIMULATION DATA". In: *The Astrophysical Journal Supplement Series* 192.1, p. 9. ISSN: 1538-4365. DOI: 10.1088/0067-0049/192/1/9. URL: http://dx.doi.org/10.1088/0067-0049/192/1/9.

Weller, J. and Lewis, A. M. (Dec. 2003). "Large-scale cosmic microwave background anisotropies and dark energy". In: *Monthly Notices of the Royal Astronomical Society* 346.3, pp. 987–993. ISSN: 1365-2966. DOI: 10.1111/j.1365-2966.2003.07144.x. URL: http://dx.doi.org/10.1111/j.1365-2966.2003.07144.x.

A Appendix

A.1 Our new model

A.1.1 Universe A

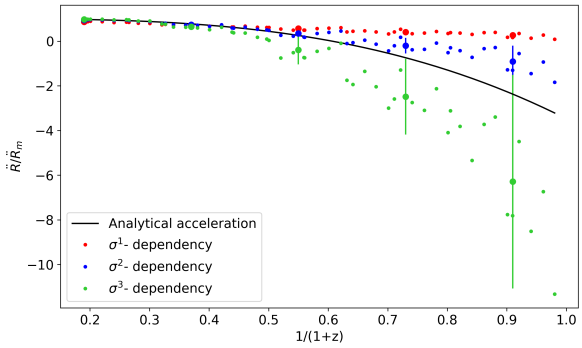

(a) *Universe A, Simulation 1.*

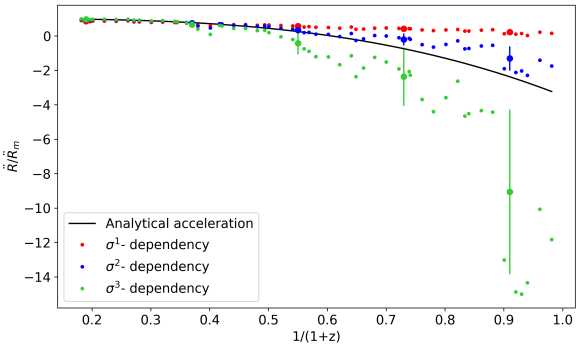

(b) *Universe A, Simulation 2.*

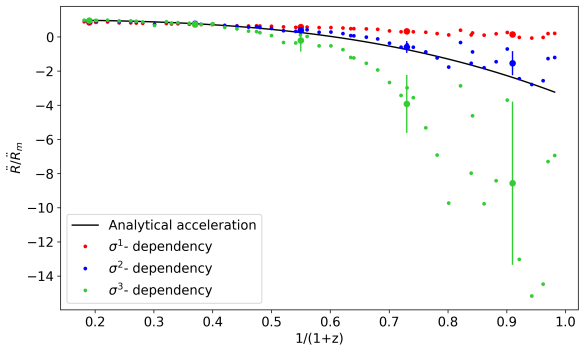

(c) *Universe A, Simulation 4.*

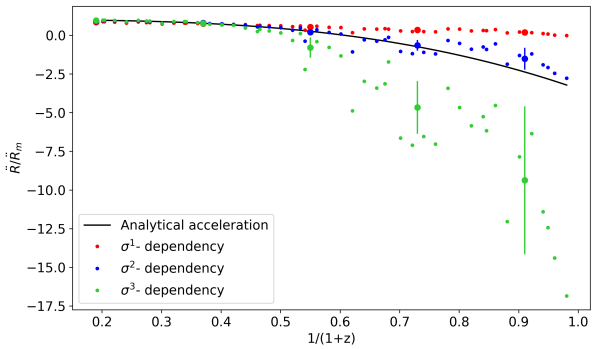

(d) *Universe A, Simulation 5.*

Figure 48: *Our new model with $x = 1, 2, 3$ for Universe A and the normalised analytical acceleration for the Benchmark model.*

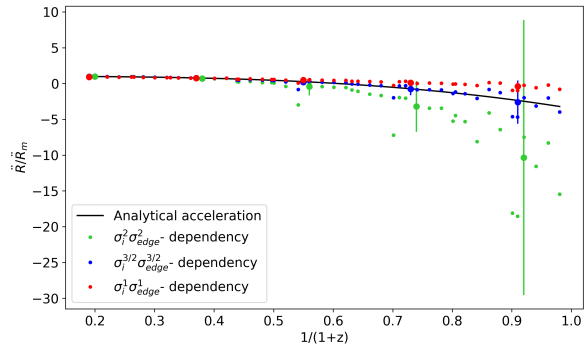

(a) *Universe A, Simulation 1.*

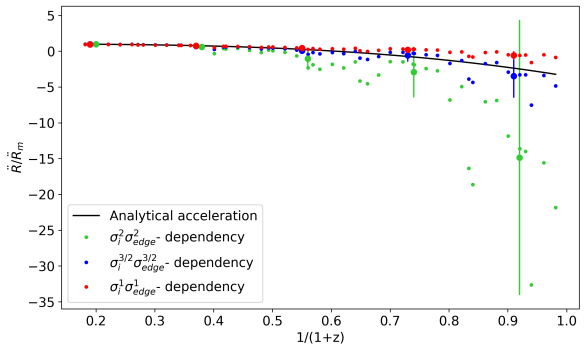

(b) *Universe A, Simulation 2.*

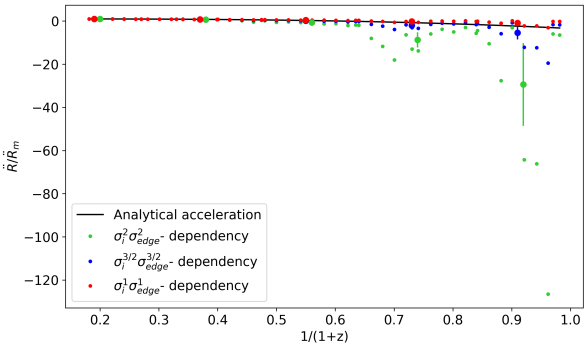

(c) *Universe A, Simulation 4.*

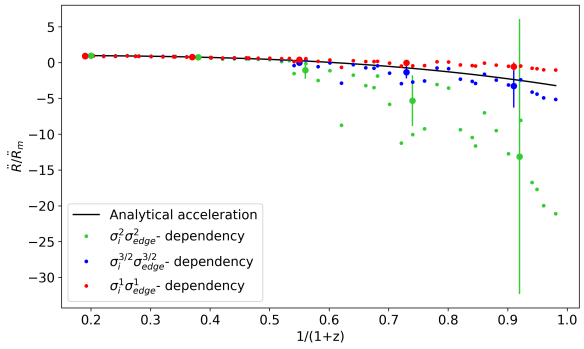

(d) *Universe A, Simulation 5.*

Figure 49: *Our extended model with $x, y = 1$, $x, y = 2$ and $x, y = 3/2$ for Universe A and the normalised analytical acceleration for the Benchmark model.*

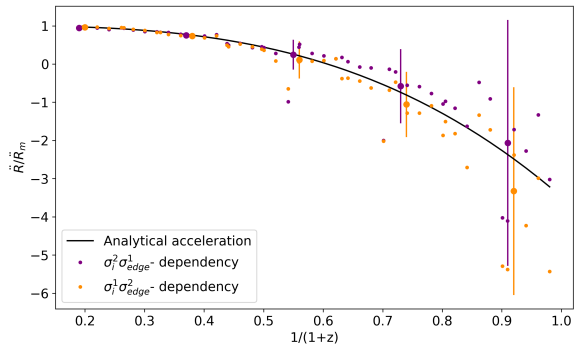

(a) *Universe A, Simulation 1.*

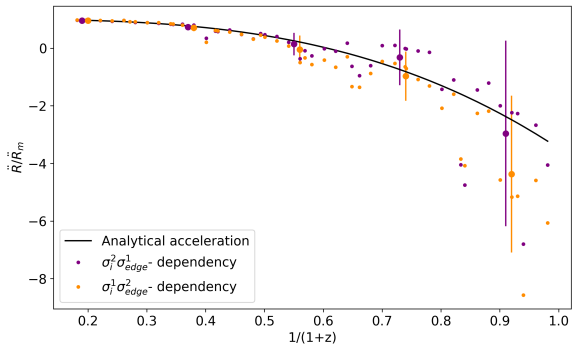

(b) *Universe A, Simulation 2.*

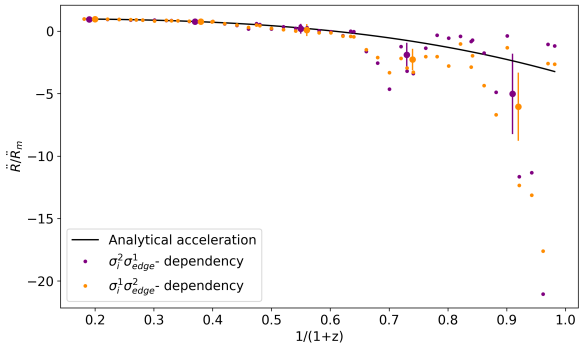

(c) *Universe A, Simulation 4.*

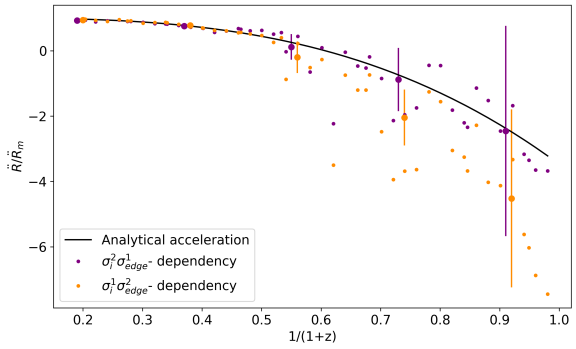

(d) *Universe A, Simulation 5.*

Figure 50: *Our extended model with $x = 2, y = 1$ and $x = 1, y = 2$ for Universe A and the normalised analytical acceleration for the Benchmark model.*

A.1.2 Universe B

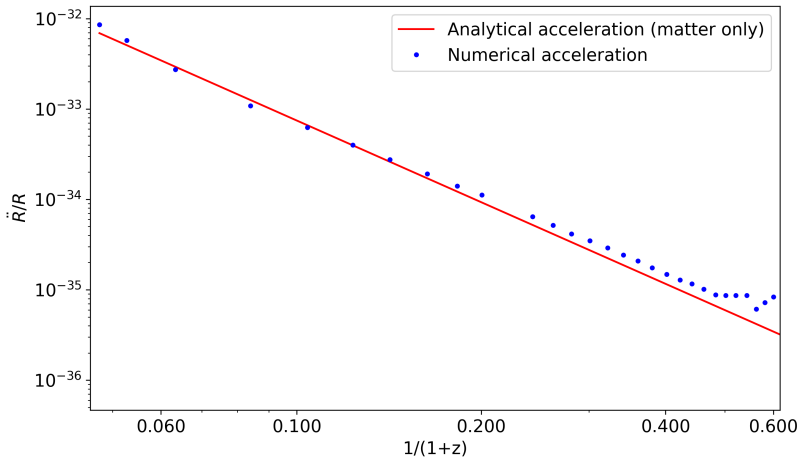

Figure 51: *The numerical acceleration for Universe B and the analytical acceleration as a function of* $1/(1+z)$ *for the Benchmark model.*

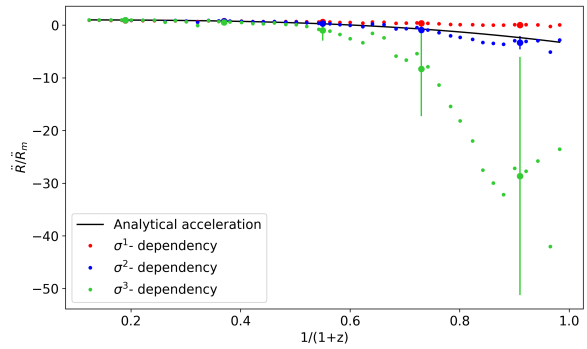

(a) *Universe B, Simulation 1.*

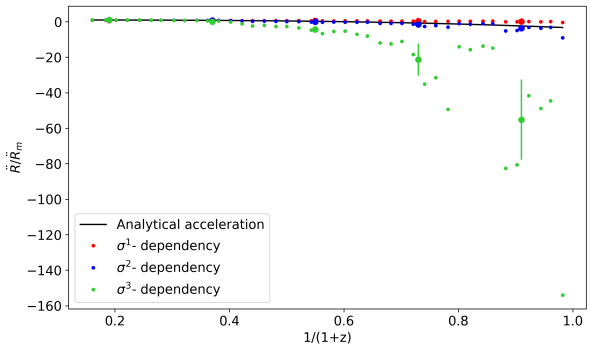

(b) *Universe B, Simulation 3.*

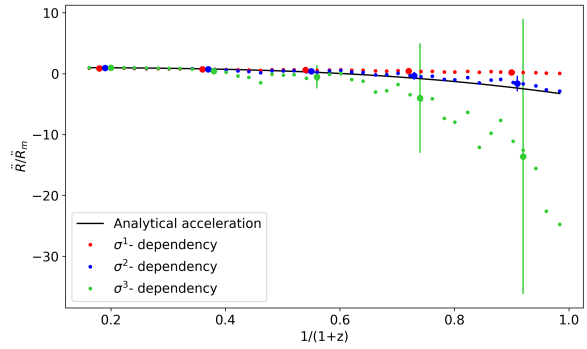

(c) *Universe B, Simulation 4.*

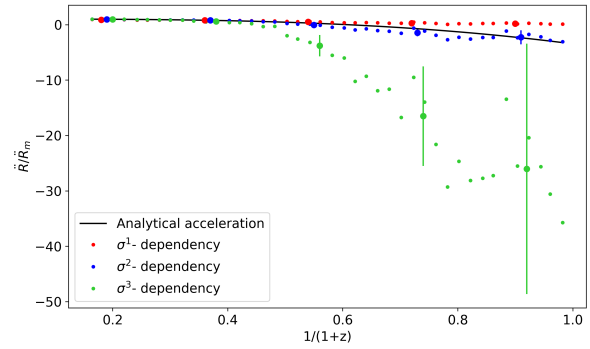

(d) *Universe B, Simulation 5.*

Figure 52: *Our new model with $x = 1, 2, 3$ for Universe B and the normalised analytical acceleration for the Benchmark model.*

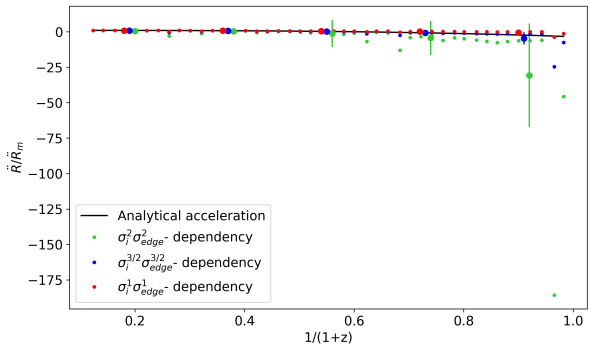

(a) *Universe B, Simulation 1.*

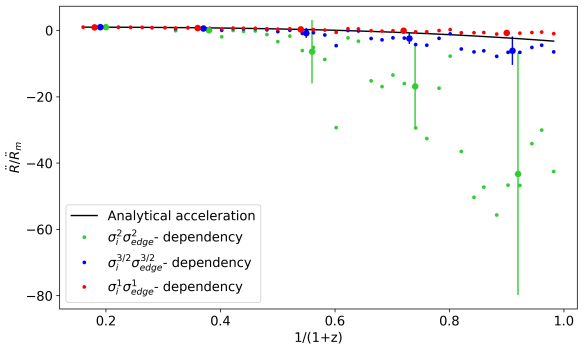

(b) *Universe B, Simulation 3.*

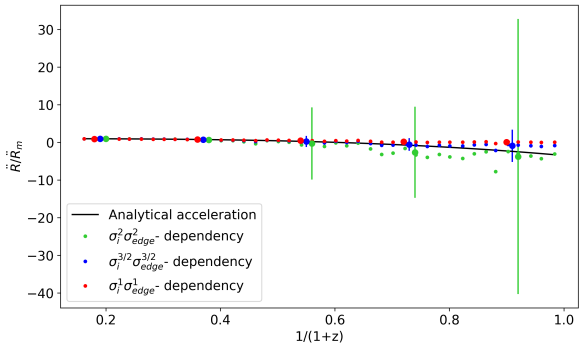

(c) *Universe B, Simulation 4.*

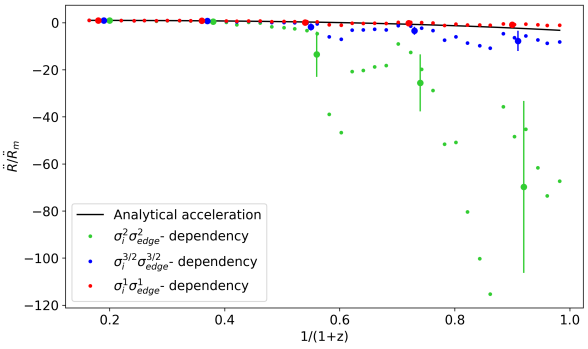

(d) *Universe B, Simulation 5.*

Figure 53: *Our extended model with $x, y = 1$, $x, y = 2$ and $x, y = 3/2$ for Universe B and the normalised analytical acceleration for the Benchmark model.*

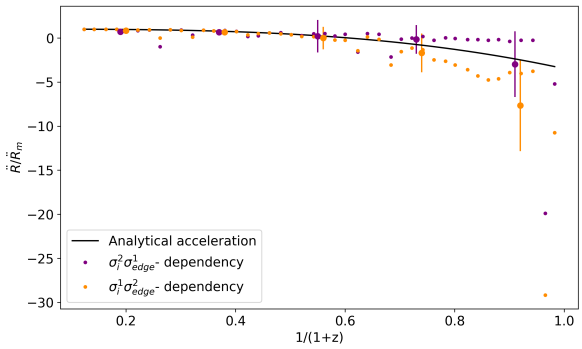

(a) *Universe B, Simulation 1.*

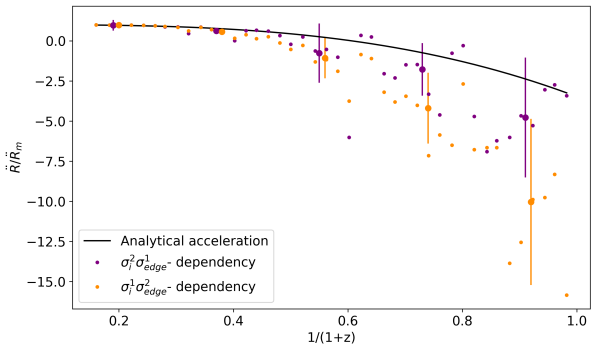

(b) *Universe B, Simulation 3.*

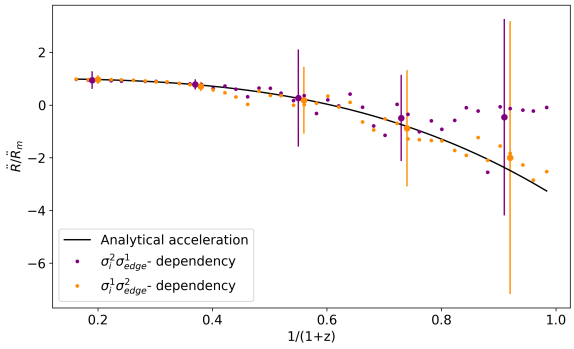

(c) *Universe B, Simulation 4.*

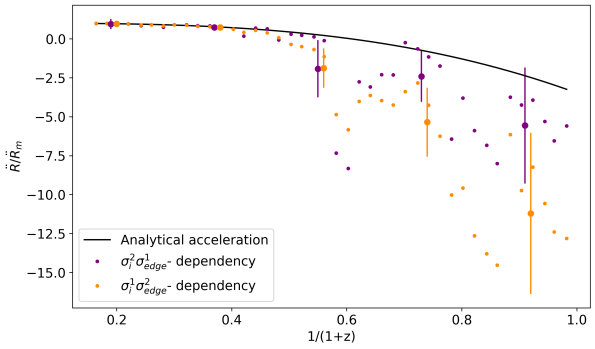

(d) *Universe B, Simulation 5.*

Figure 54: *Our extended model with $x = 2, y = 1$ and $x = 1, y = 2$ for Universe B and the normalised analytical acceleration for the Benchmark model.*

A.1.3 Universe C

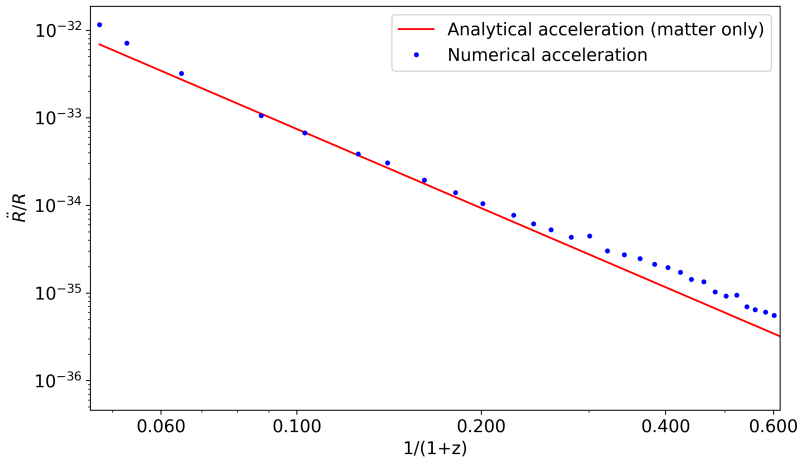

Figure 55: *The numerical acceleration for Universe C and the analytical acceleration as a function of* $1/(1+z)$ *for the Benchmark model.*

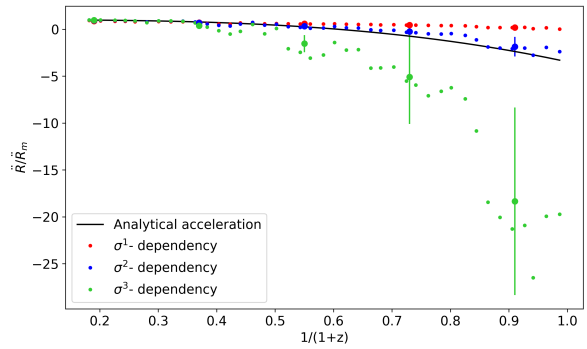

(a) *Universe C, Simulation 1.*

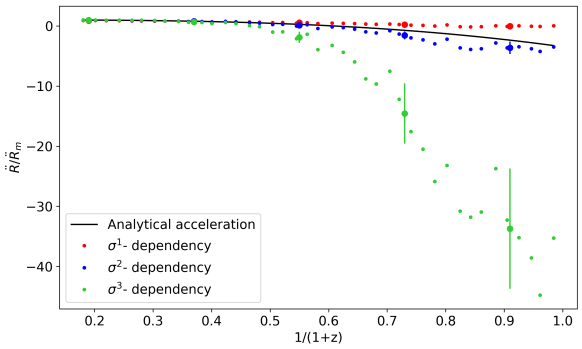

(b) *Universe C, Simulation 3.*

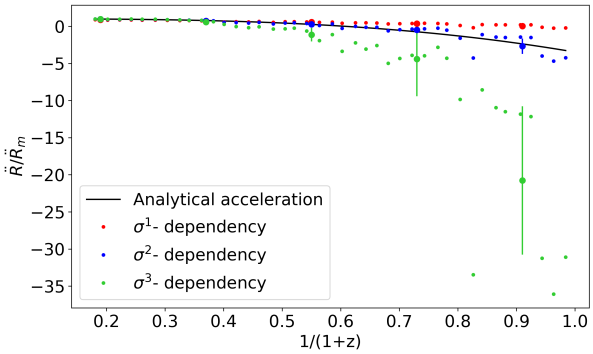

(c) *Universe C, Simulation 4.*

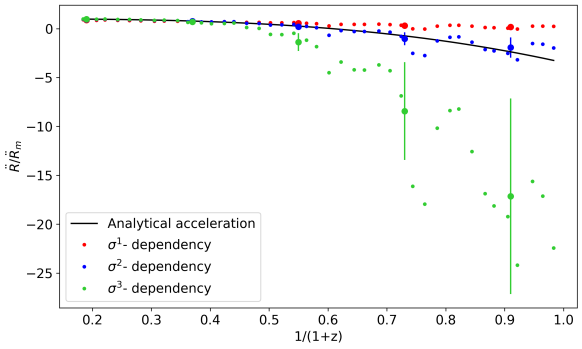

(d) *Universe C, Simulation 5.*

Figure 56: *Our new model with $x = 1, 2, 3$ for Universe C and the normalised analytical acceleration for the Benchmark model.*

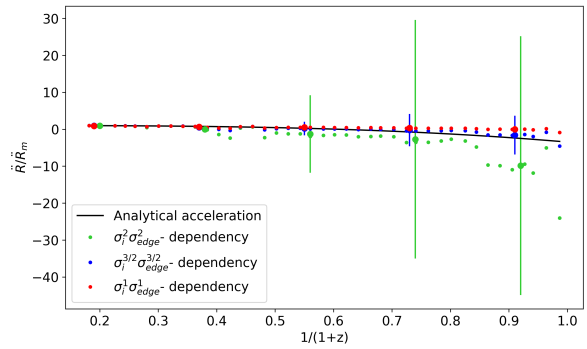

(a) *Universe C, Simulation 1.*

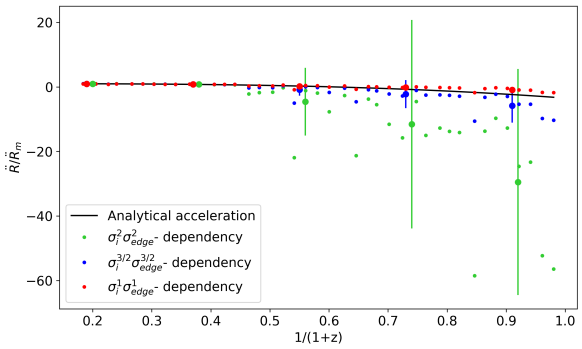

(b) *Universe C, Simulation 2.*

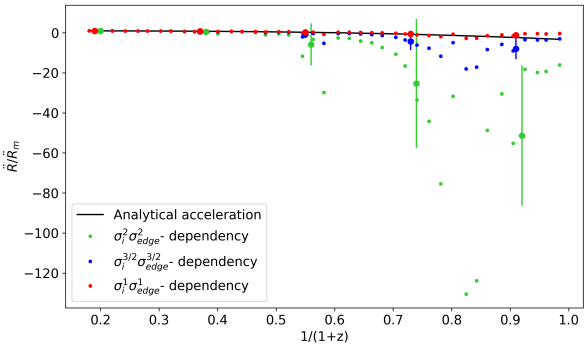

(c) *Universe C, Simulation 3.*

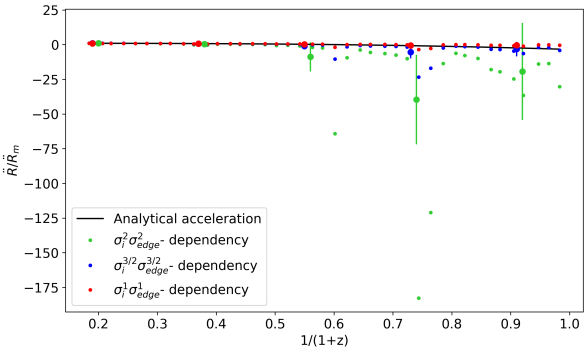

(d) *Universe C, Simulation 5.*

Figure 57: *Our extended model with $x, y = 1$, $x, y = 2$ and $x, y = 3/2$ for Universe C and the normalised analytical acceleration for the Benchmark model.*

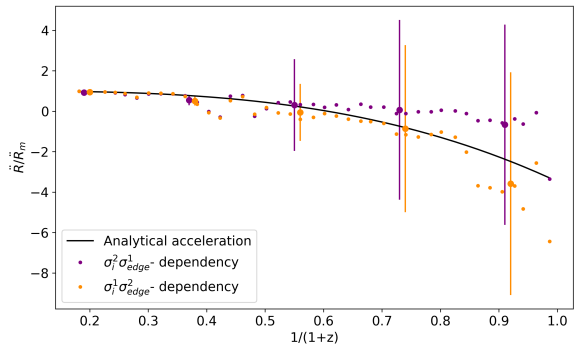

(a) *Universe C, Simulation 1.*

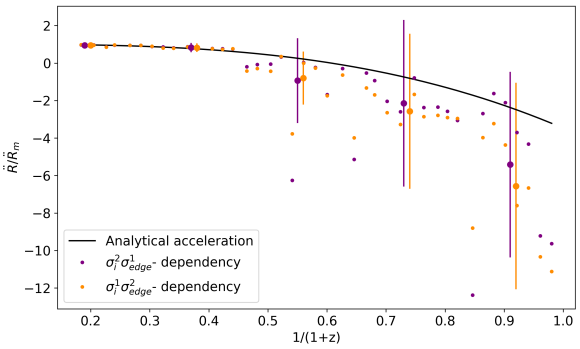

(b) *Universe C, Simulation 2.*

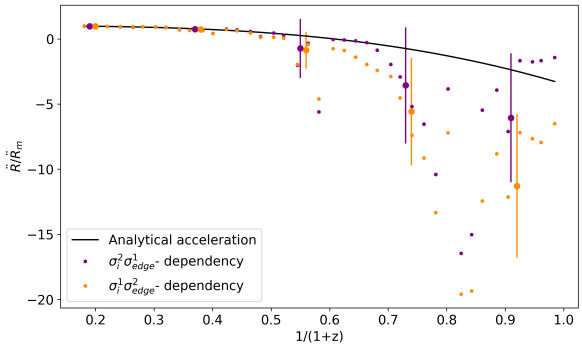

(c) *Universe C, Simulation 3.*

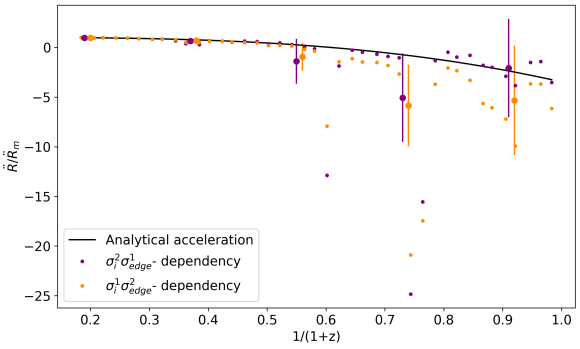

(d) *Universe C, Simulation 5.*

Figure 58: *Our extended model with $x = 2, y = 1$ and $x = 1, y = 2$ for Universe C and the normalised analytical acceleration for the Benchmark model.*